

Correcting misclassification errors in crowdsourced ecological data: a Bayesian perspective.

Edgar Santos-Fernandez

E-mail: santosfe@qut.edu.au, edgar.santosfdez@gmail.com

Erin E. Peterson

Julie Vercelloni

Em Rushworth

Kerrie Mengersen

E-mail: k.mengersen@qut.edu.au

School of Mathematical Sciences. Queensland University of Technology.

Australian Research Council Centre of Excellence for Mathematical and Statistical Frontiers (ACEMS)

Summary. Many research domains use data elicited from “citizen scientists” when a direct measure of a process is expensive or infeasible. However, participants may report incorrect estimates or classifications due to their lack of skill. We demonstrate how Bayesian hierarchical models can be used to learn about latent variables of interest, while accounting for the participants’ abilities. The model is described in the context of an ecological application that involves crowdsourced classifications of georeferenced coral-reef images from the Great Barrier Reef, Australia. The latent variable of interest is the proportion of coral cover, which is a common indicator of coral reef health. The participants’ abilities are expressed in terms of sensitivity and specificity of a correctly classified set of points on the images. The model also incorporates a spatial component, which allows prediction of the latent variable in locations that have not been surveyed. We show that the model outperforms traditional weighted-regression approaches used to account for uncertainty in citizen science data. Our approach produces more accurate regression coefficients and provides a better characterization of the latent process of interest. This new method is implemented in the probabilistic programming language Stan and can be applied to a wide number of problems that rely on uncertain citizen science data.

Keywords: Bayesian model, beta regression, corals, ecology, image classification, misclassification error, monitoring, spatial model, participants’ performance measures, the Great Barrier Reef

1. Introduction

Over the last decades, citizen science (CS) and crowdsourcing projects have become increasingly popular in several domains for tasks that require a large number of participants (i.e. volunteers or workers) to collect scientific data, generally using e-platform services (Bonney et al., 2014). These programs help overcome traditional scientific limitations by increasing the volume of data collected or processed,

while also engaging the general population in science; creating awareness and helping to reach global milestones such as the UN Sustainable Development Goals (Jordan et al., 2011; Hsu et al., 2014; Marshall et al., 2012). Hundreds of CS projects can be found, for example, at the Federal Crowdsourcing and Citizen Science Toolkit (US Federal, 2018), Zooniverse (<https://www.zooniverse.org>), iNaturalist (<https://www.inaturalist.org>) and eBird (Sullivan et al., 2009). These platforms connect millions of collaborators all over the world. However, one of the main concerns when making statistical inferences using data obtained via crowdsourcing is the inherent presence of misclassification or measurement errors resulting from participants' variable skill levels and abilities (Bachrach et al., 2012; Venanzi et al., 2014; Mengersen et al., 2017; Clare et al., 2019; Bird et al., 2014). A second concern relates to spatial dependence in the data, which has been found to produce incorrect estimates in species abundance models when it is not accounted for (e.g. Lichstein et al., 2002; F. Dormann et al., 2007). Spatial autocorrelation occurs naturally in many ecological datasets (Ver Hoef et al., 2018) and this is especially true in data collected by citizen scientists (Fritz et al., 2019), who tend to capture observations in easily accessible areas (Mengersen et al., 2017). The models developed in this study address both of these important issues.

In the ecological and environmental areas, a large body of research focuses on the estimation of unbiased species abundance and distribution relative to predictors such as habitat conditions and availability, as well as anthropogenic disturbances such as the presence of roads (Aarts et al., 2012; Fithian et al., 2015; Guélat and Kéry, 2018). Generalized linear models (GLM) and its variants are commonly used to assess whether one or more predictors are associated with a response variable (Gelfand et al., 2005; Bolker et al., 2009). However, misclassification errors in the observed variables produce biased regression coefficients and poor model estimates, which can substantially attenuate the influence of predictors in the model leading to potentially inaccurate inferences (Fuller, 2009; Muff et al., 2015). This issue is illustrated using a GLM with a beta distributed response variable via simulations in the supporting web materials section.

Approaches that pool or integrate CS elicited data with those obtained from professional monitoring programs are gathering momentum (Peterson et al., 2020). This idea revolves around meta-analysis principles and has been extensively studied in many areas including medicine, social sciences, and the environment (see Higgins et al., 2009; Claggett et al., 2014; Rice et al., 2018), as well as ecological settings (Koricheva et al., 2013). There are three general approaches used to model error-prone ecological data. In the first case, measurement error is ignored, but this approach generally produces poor estimates and is not suitable for citizen science data that is generally messy; see the supporting materials. The second approach is to use weighted linear regression (i.e. weighted approach) with observation weights proportional to the user's accuracy or performance measures (Bird et al., 2014; Peterson et al., 2020). This ensures that data from users with poorer accuracy receive lower weights in the regression model. The weighted approach may be based on fixed mechanistic weights with no variability around the values or distributions may be imposed on the weights within a Bayesian

framework to represent individual accuracies. Generally these weights are obtained using a gold standard (e.g. expert classification) or a testing dataset where the true classes/categories are known. A third method considers imperfect classification taking into consideration the user's sensitivity and specificity, denoted here as *se* and *sp* respectively. In this context, these measures refer to the ability of the citizen to correctly detect the presence (i.e. true positive) and absence (i.e. true negative) of the target species. See for example, Petracca et al. (2018).

Several variations of the second and third approaches described above rely on the Bayesian paradigm which provides a substantial number of practical and theoretical benefits (Bernardo and Smith, 2009; Hobbs and Hooten, 2015). For example, a fully Bayesian formulation of the weighted approach would include a prior distribution on the weights to capture the corresponding uncertainty of these quantities, which would, in turn, influence the other parameter estimates and associated uncertainty in the model (Choy et al., 2009). The estimation of these users' performance measures is relevant for many crowdsourced and citizen science projects where the users are trained, and potentially compensated or rewarded for their engagement, dedication and contributions (e.g. Amazon Mechanical Turk; Wiggins and Crowston, 2015; Garriga et al., 2017).

Within the occupancy modelling framework, several authors have approached the issue of bias correction by means of performance measures, especially the false-positive rates (Chambert et al., 2015; Clare et al., 2019). A recent extension suggested by Pacifici et al. (2017) also includes a spatial component in the form of a multivariate conditional autoregressive (MVCAR) prior, which accounts for spatial dependency in the data. In another example, Guélat and Kéry (2018) described residual spatial autocorrelation in the context of species distribution modelling in the presence of misclassifications. Several models that account for spatial dependency have also been developed within the Bayesian framework for citizen science data (Humphreys et al., 2019). Conditional autoregressive (CAR) priors have been found to adequately capture spatial variability in some studies (Pagel et al., 2014; Purse et al., 2015; Arab et al., 2016; Arab and Courter, 2015), while Gaussian random fields (Humphreys et al., 2019) and stochastic partial differential equations (SPDE) (Peterson et al., 2020) have been successfully used in others. To our knowledge, no one has addressed the issue of misclassification in citizen science accounting for spatial dependence.

We present a new method used to account for bias and uncertainty in crowdsourced and citizen science data, which we refer to as a spatially dependent misclassification error (SDME) approach. More specifically, we propose a Bayesian hierarchical spatial model used to correct misclassification errors and estimate the latent proportion of the target region occupied by a given species or ecological community. In the context of our case study, we are interested in estimating the percent or proportion of the seafloor covered in hard corals within an area; hereafter referred to as hard coral cover. We demonstrate the approach using simulated data and field estimates of coral cover collected within the Australian Great Barrier Reef between 2008-2017. Finally, we discuss the advantages and disadvantages of the approach, as well as the main implications of the research. In keeping with the case study,

we concentrate on the classification of images, but the methods are also applicable to the analysis of other sources such as text, video, audio, etc. found in citizen science.

1.1. *Motivating dataset: classification of coral reef images*

1.1.1. *Origins of coral reef images*

The Great Barrier Reef (GBR) is one of the richest and most complex ecosystems in the world. However, coral reefs are negatively affected by pressures such as climate change, which have caused a substantial decline in hard coral abundance (Death et al., 2012; Ainsworth et al., 2016; GBRMPA, 2014). In addition, monitoring the GBR is especially challenging because it extends over 346,000 km² and traditional marine surveys are expensive (Nichols and Williams, 2006; Roelfsema and Phinn, 2010; Nygård et al., 2016; Vercelloni et al., 2020). To address these issues, Peterson et al. (2020) demonstrated how image-based coral cover data elicited from citizens can be combined with other professional data sources to improve the spatio-temporal data coverage in the GBR and increase the information gained to inform management. This approach was operationalised in the Virtual Reef Diver project using the weighted approach (<https://www.virtualreef.org.au/>), without accounting for misclassification bias. Therefore, we developed an experiment within the Virtual Reef Diver project to further assess the potential of citizen science and crowdsourced data for monitoring coral cover. Our main purpose is to assess the participants' abilities to identify hard corals within geotagged images while determining the impact of different reef disturbances on hard coral cover changes. In addition, we want to evaluate the quality of the estimates we obtain from the experiment.

We obtained a set of $N = 1585$ images from unique locations across the GBR taken between years 2008 and 2017 by the XL Catlin Seaview Survey (González-Rivero et al., 2014) and the University of Queensland's Remote Sensing Research Centre (Roelfsema et al., 2018), which had been previously classified by marine scientists. Each image contained 40 spatially balanced, random classification points. It is common to treat classifications from coral reef scientists as the gold standard, with no uncertainty associated with the measurements. However, ecologists are often interested in data from large regions where it is infeasible to obtain estimates of the proportion of hard corals (y_j) for large volumes of images due to time and financial constraints. In these cases, citizen science and crowdsourcing are excellent alternatives (Dickinson et al., 2010).

1.1.2. *Spatial covariates for coral cover*

Four spatial covariates representing reef disturbances, management zones, and continental reef-shelf position were considered in the model (Table 1). Reef disturbance covariates were sourced from Matthews et al. (2019). The maximum value of Degree Heating Weeks (DHW) is generally used to represent a reef's thermal stress and has been found to be associated with episodes of coral bleaching (Hughes et al., 2018a). Exposure to cyclones is defined as the number of hours with potentially damaging waves (height > 4m) during tropical cyclones or storms (Puotinen et al., 2016). Note that,

Table 1. Covariates included in the model.

Covariate	Variable	Description	Source
DHW	continuous	Degree heating weeks (max DHW/year). It is a proxy for bleaching severity.	Hughes et al. (2018a); Matthews et al. (2019)
no_take	binary {no-take = 1, take = 0}	No-take marine reserves where fishing is not allowed.	GBRMPA (2014)
shelf	categorical {middle = 0, outer = 1}	Position of the reef. For these images we had no inner reefs.	GBRMPA (2014)
CYC	continuous	Cyclone effect measured as cumulative hours of exposure to waves greater than 4m (4MWh/year).	Puotinen et al. (2016); Matthews et al. (2019)

nearest neighbour interpolation was used to fill in locations where covariate values were missing.

We assume that images in close proximity within the same reef habitat are more likely to have a similar proportion of hard coral than those situated in a different habitat, motivating the use of a spatial component in our models. Spatial autoregressive models (Ver Hoef et al., 2018) or SPDEs (Lindgren and Lindgren 2011) are often used to model large datasets because they are more computationally efficient than geostatistical models applied to spatially continuous point-referenced data (Cressie and Wikle 2011). Therefore, we generated a set of Voronoi polygons using the image locations as centroids and boundaries based on Euclidean distance (Okabe et al., 2009; Gold, 2016), which we then used to define the spatial domain in the model. Two polygons are neighbors if they share a common boundary. The example in Fig 1 shows a Voronoi diagram with the spatial proportion of hard coral on the edges of a reef from Heron Island, Australia. This diagram is superimposed on a background satellite image obtained from Google. The black and red and points represent the locations where images were taken, while the blue ones represent locations of interest for reef management purposes where an estimate of the proportion of hard corals are required. The images capture an extent over a certain area of the reef defined by transects.

2. Materials and methods

2.1. Survey design and description of the classification task

For each image, we obtained the proportion of five benthic categories (i.e. hard and soft coral, algae, sand, and other). The images were clustered into groups based on proportions of each of the five categories using the K-Means clustering algorithm included in the *stats* package in R. This approach produced three clusters of images based on their benthic composition: (1) images mostly composed of hard corals, (2) largely dominated by algae, and (3) predominantly composed of soft corals.

Then, a random sample of 514 images was selected from the clusters ensuring that we had coverage across the camera types used to take the images, which had different resolutions (Canon, Lumix, Olympus, Sony and Nikon). This design ensured that the images represented the benthic composition and camera types found in the full set of images, as well as a wide spectrum of classification difficulties. We randomly selected 30% of the 514 images ($n = 171$) and assumed the corresponding proportion

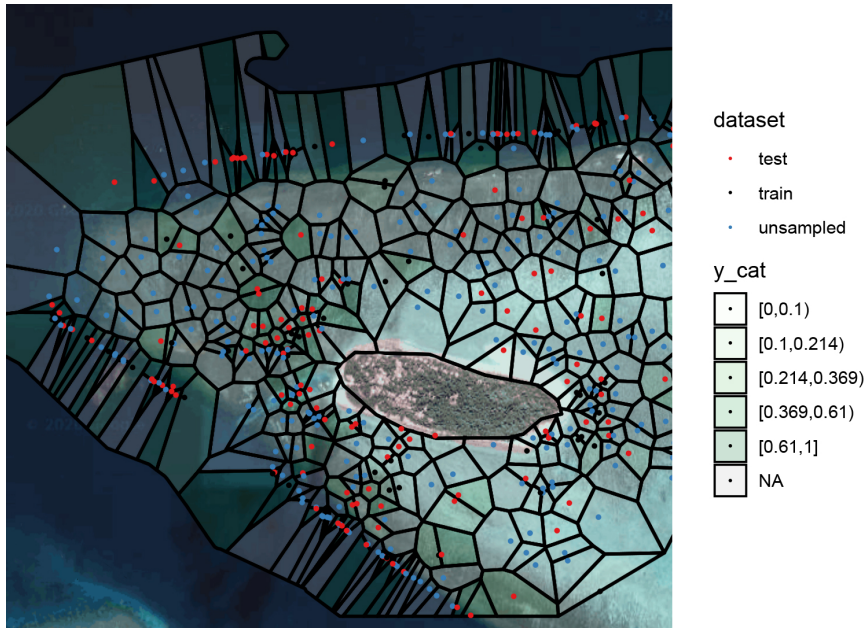


Fig. 1. Voronoi diagram of hard coral cover around Heron Island, Australia. The categorical colors are the classes obtained using the quintiles of the hard coral proportion obtained by expert elicitation. The dots represent the location of the measurement. Black and red dots are locations where images were taken and in images given by the black dots the latent true proportion is available. Blue dots in Voronoi areas are positions on the reef in which we want to predict the coral cover.

of hard corals y to be known (i.e. training dataset) as the result of elicitation by the coral reef scientists. For the remaining 343 images (i.e. testing dataset), we assumed the proportion of hard corals was unknown and must be estimated from the model based on the participants' responses. This combined dataset of 171 known values of y and 343 estimated values of y was then used to estimate the model parameters. Finally, we treated the 1071 remaining image locations as an unsampled/prediction dataset, which allowed us to predict coral cover using the fitted model and also validate the model results.

There exists a trade-off between survey costs and the quality of the estimates (e.g. participants' performance measures) and knowing 30% of the labels is generally considered suitable for these kind of problems. This and other training partitions have been found suitable in the literature. See e.g. Pacifici et al. (2017) who consider 25% and 50% values, while Chambert et al. (2018) deal with smaller proportions such as 5, 10, 20 and 30%.

The 514 images were displayed for classification on Amazon Mechanical Turk (<https://www.mturk.com/>) and workers were asked to classify points into five benthic categories (i.e. hard coral, soft coral, algae, sand, and other). We created a help file showing underwater image classification to train the participants, which described the characteristics of the benthic categories (https://github.com/EdgarSantos-Fernandez/reef_misclassification/blob/master/HelpGuide_MTurk2020200203.pdf). Participants also had to pass a qualification test by achieving a score of at least 60% to perform classifications, which is a common mechanism of quality control (Rashtchian et al., 2010). Classification

data were collected from 2020-Jan-14 to 2020-Feb-12.

Participants were paid 0.10 USD per completed image, which equates to more than the U.S. federal minimum wage (\$7.25 per hour). The number of images classified by each participant varied because they were free to cease the task at any time. Participants were assigned a sequence of images from the list of 514 obtained by random sampling without replacement.

For each image, they were asked to classify 15 (out of the 40) random points and the task could only be submitted after classifying all the points on an image. The structure of the data will be discussed below in Fig 4. We considered asking participants to annotate the full 40 points per image, but we were concerned that it would be too exhausting for the participants and would reduce participation. In addition, Beijbom et al. (2015) showed that accurate image-based estimates of coral cover could be obtained with approximately 10 points per image, and that manual classification of additional points by marine scientists did not substantially improve coral cover estimates for an individual image. Fig. 2 shows one of the underwater images taken from Heron Island Reef. The true classes are shown for the 15 spatially balanced random points classified by a participant.



Fig. 2. Underwater image from Heron Island Reef Management Area, Great Barrier Reef, Australia. It shows 15 spatially balanced random points elicited by a marine scientist. The color of the circle represents the true benthic category, which is defined as the class with the highest proportion within the area delimited by the circle.

Once data were submitted by workers, some exclusion rules were put in place to discard non-informative data, careless and non-genuine users, and software bots. This was done by using the values of coral cover from the training dataset. Subjects with accuracy values lower than 40% in the training images were excluded. We also considered other indicators including the number of classifications per hour and inconsistencies on some of the fields of the database tuples. Failing to remove these noisy data points generally results in biased estimates. Thus, the final dataset used for the case study comprised classifications from 157 subjects and included 212,910 observations (i.e. classification points) and 14,194 image classifications.

Fig. 3 shows an example of the elicitations from two subjects with different abilities to classify hard coral. We found that images with a large proportion of algae tended to produce larger false-positive rates compared to (easier) images with a large portion of sand. This is probably because algae look like hard corals to less proficient subjects.

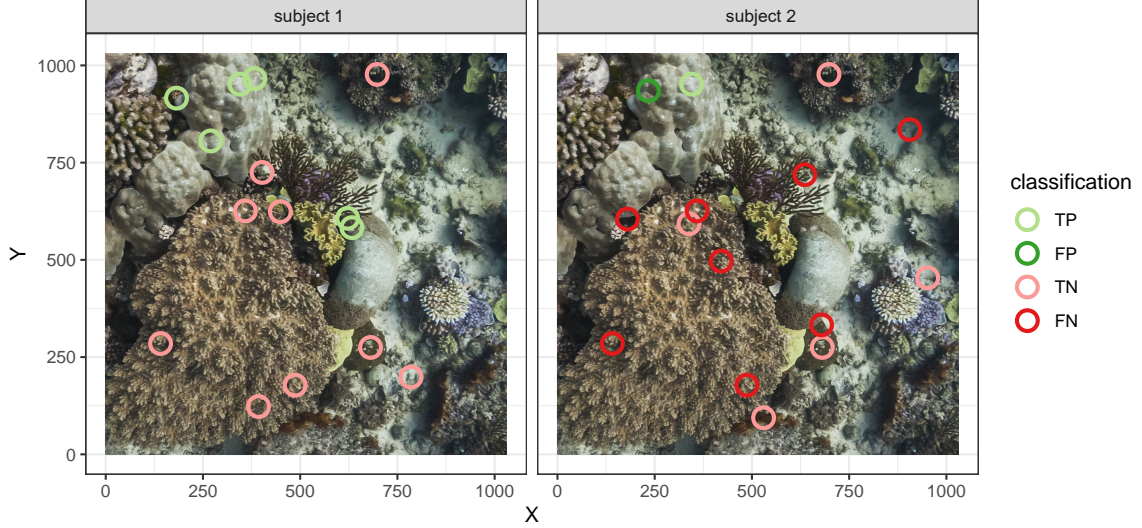


Fig. 3. Example of an image classified by two subjects with different abilities to classify corals. Each image contains $q = 15$ random classification points that are colour coded to represent whether hard coral has been classified correctly (true positive). Dark colours represent misclassification (dark green = false positive (FP), dark red = false negative (FN)). Light colours represent correct classifications (light green = true positive (TP), light red = true negative (TN)).

2.2. Statistical description of the classification task

In this section, we provide a statistical description of the classification task, the misclassification errors and accuracy, and the spatial Bayesian hierarchical model. A complete list of symbols and definitions has been provided in the Appendix section that readers can refer to.

Consider coral reef images taken at geographic locations defined by latitude and longitude (lat and lon). Let these locations represent the centroids of Voroni polygons used to define areal units.

The presence or absence of the target class (hard corals) in a subset of points is obtained within each image. We denote y as the true proportion of these points containing the target class.

In binary image-classification tasks, participants are asked whether each of q sample points contain the class of interest. In the case study described above, $q = 15$ and the target class is hard corals. This approach is also known in ecology as random point count methodology (Kohler and Gill, 2006). Let $z_{ijk} = \{0, 1\}$ with “1” denoting the target class, in the point k from the j^{th} image classified by the i^{th} subject. Thus, there might be a disagreement between the elicited and the true latent class. For a given image j , the *apparent* proportion of the target species (\hat{y}_{ij}) is obtained as the sum of points

that are labeled as “1” divided by q .

$$\hat{y}_{ij} = \sum_{k=1}^q z_{ijk}/q \quad (1)$$

2.3. Characterization of misclassification errors and participant's accuracy

The performance of the i^{th} subject is measured by their sensitivity (se_i), specificity (sp_i) and accuracy(acc_i), which are obtained as follows:

$$se_i = \frac{\sum_{j=1}^m \sum_{k=1}^q TP_{ijk}}{\sum_{j=1}^m \sum_{k=1}^q TP_{ijk} + \sum_{j=1}^m \sum_{k=1}^q FN_{ijk}}, \quad (2)$$

$$sp_i = \frac{\sum_{j=1}^m \sum_{k=1}^q TN_{ijk}}{\sum_{j=1}^m \sum_{k=1}^q TN_{ijk} + \sum_{j=1}^m \sum_{k=1}^q FP_{ijk}}, \quad (3)$$

and

$$acc_i = \frac{\sum_{j=1}^m \sum_{k=1}^q TP_{ijk} + \sum_{j=1}^m \sum_{k=1}^q TN_{ijk}}{\sum_{j=1}^m \sum_{k=1}^q TP_{ijk} + \sum_{j=1}^m \sum_{k=1}^q FN_{ijk} + \sum_{j=1}^m \sum_{k=1}^q TN_{ijk} + \sum_{j=1}^m \sum_{k=1}^q FP_{ijk}}, \quad (4)$$

where for the k^{th} point on the j^{th} image classified by the subject i , the four indicator variables $TP_{ijk}, TN_{ijk}, FP_{ijk}, FN_{ijk}$ are equal to 0 or 1, with $TP_{ijk} = 1$ if the point is correctly classified as positive given that the target species is present (true positive) and $TN_{ijk} = 1$ if the point is correctly classified as negative when the target species is absent (true negative). The false positive $FP_{ijk} = 1$ when the point is incorrectly classified as positive when the target species is absent and the false negative $FN_{ijk} = 1$ occurs when it is misclassified as not present when the target species is present in the location. For a discussion on the 2×2 confusion matrix in the ecological context see Manel et al. (2001); Vayssières et al. (2000).

Accounting for a proportion of locations where the y_j is known, informs the model as a training set about the users' abilities in terms of se_i and sp_i . This will narrow the uncertainty around the latent values in locations where the truth is unknown and contribute to model identifiability.

We will see later in Eq. 5 that the participant's performance plays a vital role in the model. Accuracy estimates from previous citizen science studies have ranged between 70 and 95% (Kosmala et al., 2016), with a subject's classification performance affected by commitment, effort, ability and selected demographic factors.

Within the Bayesian framework, se_i and sp_i for each participant are assumed to follow a probability distribution with parameters that reflect published estimates. Other potential cases consider distributions for each participant i and each image j (se_{ij} and sp_{ij}) or consider se_i and sp_i to be a mixture of distributions for easy and hard images for example. Here we adopt informed beta distributions with relatively large shape α_i and small scale β_i , which produces a density with mass closer to 1 than to 0 with a relatively small variance.

2.4. The SDME and the weighted Bayesian hierarchical model.

Participants with limited training may find it difficult to correctly identify some of the benthic categories found at the sample points. The statistic \hat{y}_{ij} gives the apparent proportion of hard corals in the images $j = 1, 2, \dots, m$ classified by the subjects $i = 1, 2, \dots, n$ and it is obtained deterministically based on the subject se_i and sp_i distributions and the true latent proportion y_j according to Eq 5 (e.g. Vose, 2008). A graphical representation of the image classification process is given in Fig 4.

$$\hat{y}_{ij} = y_j \times se_i + (1 - y_j) \times (1 - sp_i) \quad (5)$$

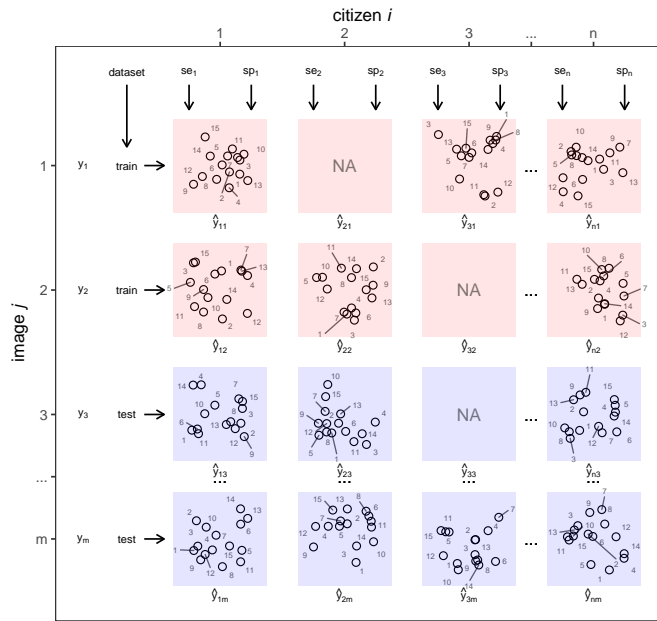


Fig. 4. Structure of the data. Tiles represent the image j (rows) being classified by the subject i (columns) with se_i and sp_i . On each classification 15 points are elicited producing estimates of \hat{y}_{ij} . Images in red are those used for training while the blue ones give the testing subset. A tiles with NA means that the image j was not classified by the subject i .

The SDME model is depicted in the directed acyclic graph in Fig. 5, which contains two plates: one for the image part (j) and the other representing the subjects (i).

When the target class of interest is absent at all of the points in the j^{th} image ($y_j = 0$), the apparent proportion y_{ij} is the false positive rate of the subject i , i.e., $y_{ij} = 1 - sp_i$. If participant i has a small sp_i , the participant will report larger values \hat{y}_{ij} for small values of y_j . When the target class is present in all the points ($y_j = 1$), the apparent proportion will be equal to the subject's sensitivity $\hat{y}_{ij} = se_i$.

The true proportion of the target class y_j within the image j is modelled in our case using a beta regression approach (Ferrari and Cribari-Neto, 2004), which is a common practice in reef modelling (e.g. McClanahan et al., 2019; Mellin et al., 2019; Peterson et al., 2020):

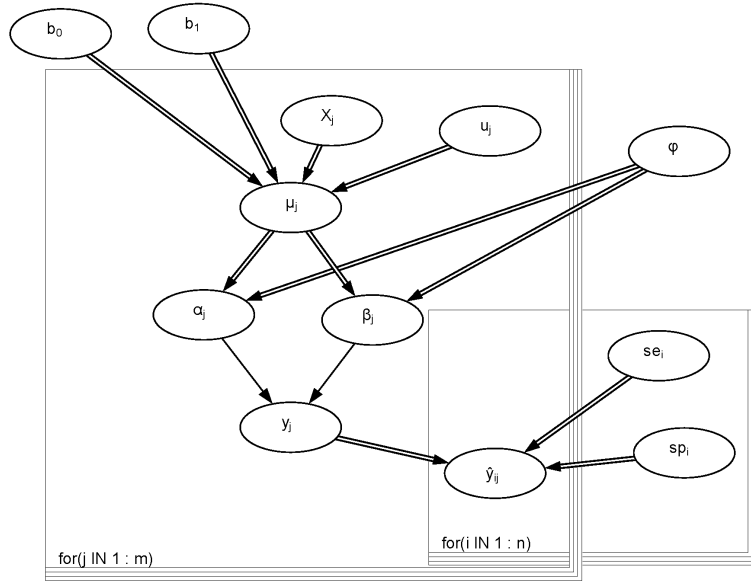


Fig. 5. Directed acyclic graph of the SDME model. Ellipses represent the stochastic/constant nodes. Solid and hollow arrows (edges) give stochastic and logical dependence, respectively. Plates represent the repeated elements. The left plate is indexed in j representing the portion of the model relating to images, while the portion relating to the workers is shown in the right plate and is indexed in i . For example, se_i is indexed in i ($i \in 1 : n$) indicating the sensitivity of users from 1 to n .

$$y_j | \alpha_j, \beta_j \sim \text{Beta}(\alpha_j, \beta_j)$$

where α_j and β_j are the shape and the scale parameters respectively. We parametrized the model based on the mean μ_j and a common precision parameter ϕ , where $\alpha_j = \mu_j \phi$ and $\beta_j = -\mu_j \phi + \phi$. The mean is conditional on the latent model, $\mu_j = \text{E}[y_j | \alpha_j, \beta_j]$, and the variance $\text{Var}(y_j) = \frac{\mu_j(1-\mu_j)}{(1+\phi)}$, where ϕ is inversely proportional to the variance of y_j .

The spatial beta regression for each image/unique location $j = 1, 2, \dots, J$ can be expressed as follows:

$$\text{logit}(\mu_j) = X_j b + u_j + \varepsilon_j, \quad (6)$$

where the matrix X_j represents a group of covariates, b is the vector of regression coefficients, ε_j is unstructured noise and u_j is a spatial component obtained from a spatial autoregressive model such as the conditional autoregressive (CAR) model prior (Besag et al., 1991; Ver Hoef et al., 2018). In a CAR model, the value at $u_{l=1,2,\dots,m}$ conditional on the first-order neighbours is the average of the n_l first-order neighbours plus Gaussian noise.

$$u_l | u_t, \tau_u \sim \mathcal{N} \left(\frac{1}{n_l} \sum_{l \sim t} u_t, \frac{1}{\tau_u n_l} \right), \quad (7)$$

where $l \sim t$ means l and t are neighbours and $l \neq t$. This prior has been implemented in Stan (Morris et al., 2019).

The Bayesian weighted model is shown in Fig. 6. In this model, the node acc_i is the subject i classification accuracy defined above in Eq. 4, which is used to weight the values of μ_{ij} in the regression model. We model acc_i using a beta prior distributions obtained from the training dataset.

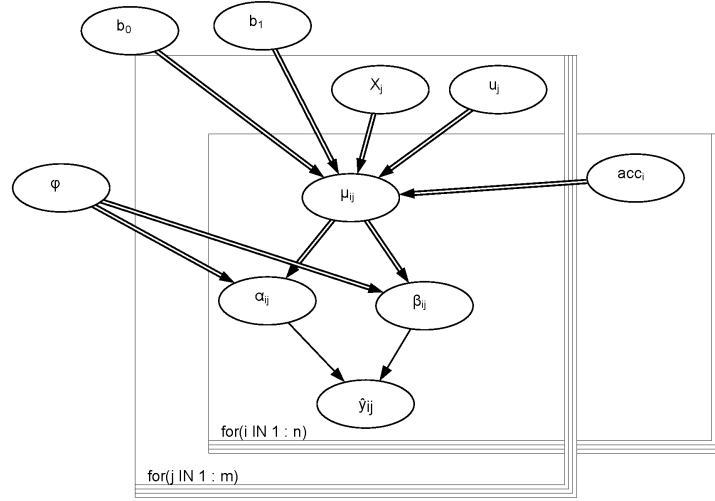


Fig. 6. Directed acyclic graph of the weighted model.

3. Simulation study

In order to assess how well the model parameters are estimated, we simulated 300 datasets and compared the fit using the weighted and the SDME models. In the SDME model, the aim was to estimate the parameters from Eq. 5 and 6: $\theta_{SDME} = \{y_i, b_0, b_1, se_i, sp_i, \phi\}$ using the apparent proportion $\hat{y}_{ij} = (\hat{y}_{11}, \hat{y}_{12}, \dots, \hat{y}_{nm})$, some available y_j values and a covariate $X = [x_1, x_2, \dots, x_j]$. In the weighted model, we estimated $\theta_w = \{\hat{y}_{ij}, b_0, b_1, acc_i, \phi\}$.

We also wanted to obtain the posterior estimates of y_i for unobserved locations j where no images were taken, where \hat{y}_{ij} is missing for all participants $i = 1, 2, \dots, n$. The simulation steps are detailed below, followed by a discussion of parameter choices.

- (a) Consider 225 points on a unit square with lat and lon on a plane representing a section of a reef. We select 80% of these points and take one image at each point. We define Voronoi cells based on Euclidean distance using the centroids defined by the lat and lon .
- (b) Assume a continuous covariate $x_j \sim N(\mu_x = 0, \sigma_x)$ sampled at the locations where the images were taken. It represents a reef disturbance and is highly associated with y_j . In the context of the case study this could represent a change in water temperature (e.g. DHW).
- (c) Fix an intercept $b_0 = 1$ and a slope $b_1 = -2$. These values are arbitrarily chosen for the purpose of the simulation study and other values do not seem to affect the results.
- (d) Include 20 subjects from 4 groups with different levels of accuracy (1-4): experienced, good, average and beginner. We assume performance measures based on the ranges reported in Kosmala

et al. (2016) and hence randomly sample beta distributions for the se_i with mean values according to the expertise membership: $se_1 = 0.99$, $se_2 = 0.95$, $se_3 = 0.90$ and $se_4 = 0.80$ and using a precision $\phi_{se} = 50$ based on the beta distribution parametrization discussed in Section 2.4. Similarly we set the mean sp values: $sp_1 = 0.99$, $sp_2 = 0.90$, $sp_3 = 0.80$ and $sp_4 = 0.70$ and use a precision $\phi_{sp} = 50$. This ensures that for every subject the probability of correctly classifying each point is stochastic.

Apart from the experienced subjects (group 1), the others have a larger false positive rate than false negative rate ($sp_i < se_i$, for $i = \{2, 3, \dots\}$). Images are classified by at least 5 participants and the probability of an image being classified by 5, 6, \dots or 20 participants is the same. Every user classified approximately 3/4 of the total number of images. In the SDME model, informative beta priors are used for se_i and sp_i , with shape parameters calculated using the mean and variance obtained from the training dataset.

- (e) Set the beta precision parameter $\phi = 30$. Compute the beta distribution mean (Eq 6) based on the spatial regression equation. Compute also the shape and scale parameters (α_j, β_j).
- (f) Simulate latent responses y_j for $j = 1, 2, \dots, m$, and based on these compute the apparent responses \hat{y}_{ij} for $i = 1, 2, \dots, n$ and $j = 1, 2, \dots, m$.

- (g) There is missingness in both y_j and \hat{y}_{ij} (Fig 7). This yields the three datasets structures that are commonly encountered in CS ecological research. The first split is whether samples or images being collected at the given locations and the images have been classified (is \hat{y}_{ij} available?), while the second depends on the underlying truth (y_j) being available. Define a vector $d_j = \{0, 1\}$ with $j = 1, 2, \dots, m$ where $d_j = 1$ if y_j is observed and $d_j = 0$ otherwise. Let also $\hat{d}_j = \{0, 1\}$, associated to \hat{y}_{ij} , where $\hat{d}_j = 1$ indicates that at least one subject has classified the image j .

In dataset 1 (i.e. training) both \hat{y}_{ij} and y_j are available and $d_j = \hat{d}_j = 1$. We randomly selected 67 images (30%) where the true proportion (y_j) is known with certainty. The second dataset (i.e. testing) is represented by those locations where images were collected and will be classified (known \hat{y}_{ij} , $\hat{d}_j = 1$), but the ground truth is not available (unknown y_j , $d_j = 0$).

Finally, we consider 45 locations (20%) that have not been sampled yet and thus there are no images, so both \hat{y}_{ij} and y_j are missing (i.e. unsampled dataset, $d_j = \hat{d}_j = 0$). We predict the proportion of the target species in these locations where no data have been collected using neighboring information and covariates.

- (h) For the study, we generated a Voronoi grid of size 15×15 spatial locations points on a unit square ($[0,1] \times [0,1]$) corresponding to the positions where the images were taken.

The simulated proportion of hard corals at the 225 locations is shown in Fig. 8(a) and spatial association between adjacent areas is evident. In the 45 unsampled locations we set \hat{y}_{ij} to missing as described above (8b; gray polygons and blue labels).

For a better understanding of the influence of the performance measures, we show \hat{y}_{ij} as a function of the true latent variable y_j for the four groups of subjects in Fig. 9. The diagonal black solid line

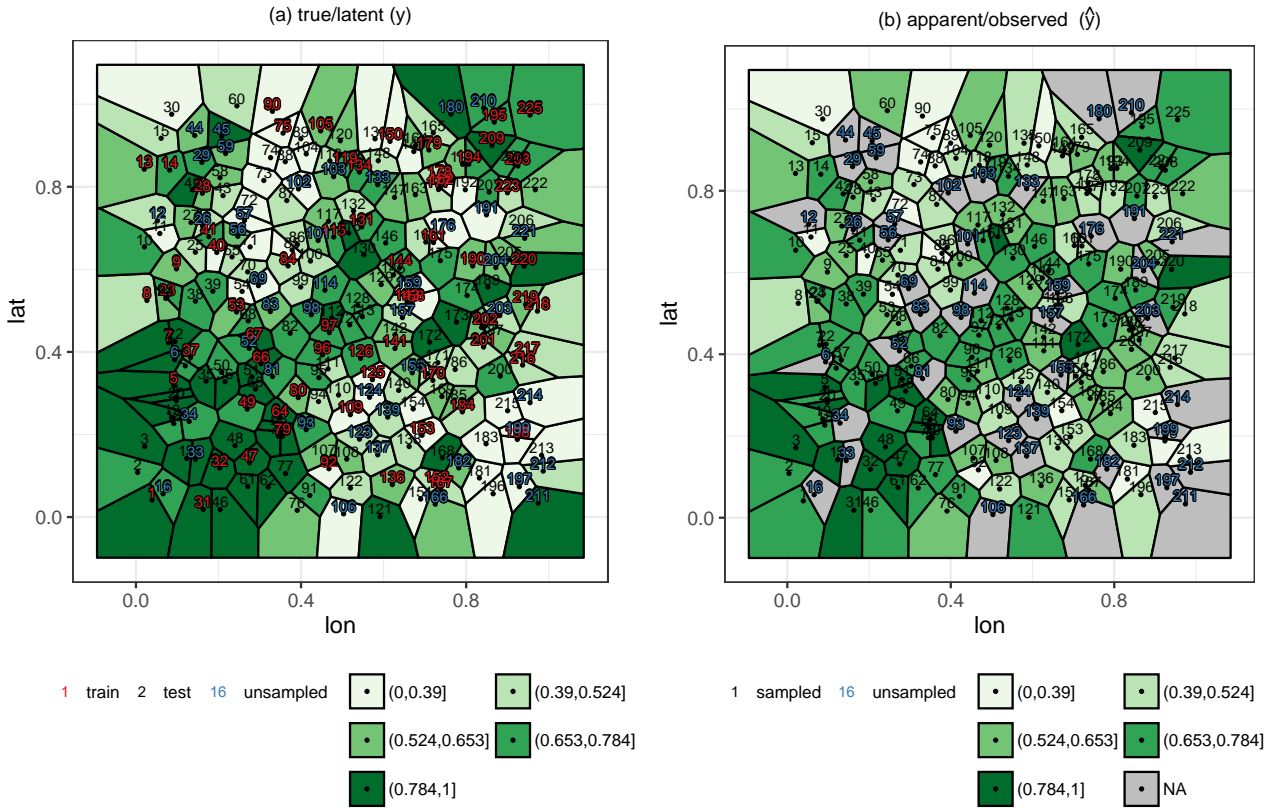


Fig. 8. (a) Voronoi diagram of the true latent proportion (y_j) at 225 simulated locations. Each Voronoi cell or polygon has a centroid represented by a point and each point is labelled from 1 to 225 in which the color represents the type of dataset (train, testing, unsampled). The true value y_j is known at 67 locations (red labels). The 45 polygons with blue labels are the unsampled locations. Black labels represent polygons from the testing dataset. The green color categories are obtained using the quintiles. (b) Voronoi diagram of the apparent proportion of coral cover (\hat{y}_{ij}) elicited by the subjects. Missing values in \hat{y}_{ij} are shown in (gray polygon with text in blue). There are 45 mismatches (out of 80 locations) in the proportion categories in (a) and (b): 1, 2, 8, etc. since users mostly overestimated the proportion of species.

precision parameter in the beta distribution ($\phi \sim \mathcal{N}(20, 5)T[10, 60]$). Details of the model are given in Fig.11. The Stan code for the SDME model is provided in the supporting materials.

3.2. Simulation results

The SDME model captured the true parameter values much better than the weighted model (Table 2). The estimates for ϕ are off in the weighted model and the SE of the mean and 95% density intervals are narrow. The intervals are wider for SDME, but they capture the true parameters' values.

The posterior densities and trace plots for the regression coefficients show well mixed chains and apparent convergence (See the supporting materials) and the R-hat convergence diagnostic (Gelman et al., 1992; Vehtari et al., 2019) produced values well below 1.1. The posterior values of se_i and sp_i values were equally well retrieved for most of the subject groups (also in supporting materials).

Fig. 12 (c) depicts the degree of success in retrieving the true latent proportion (y_j). The diagram in

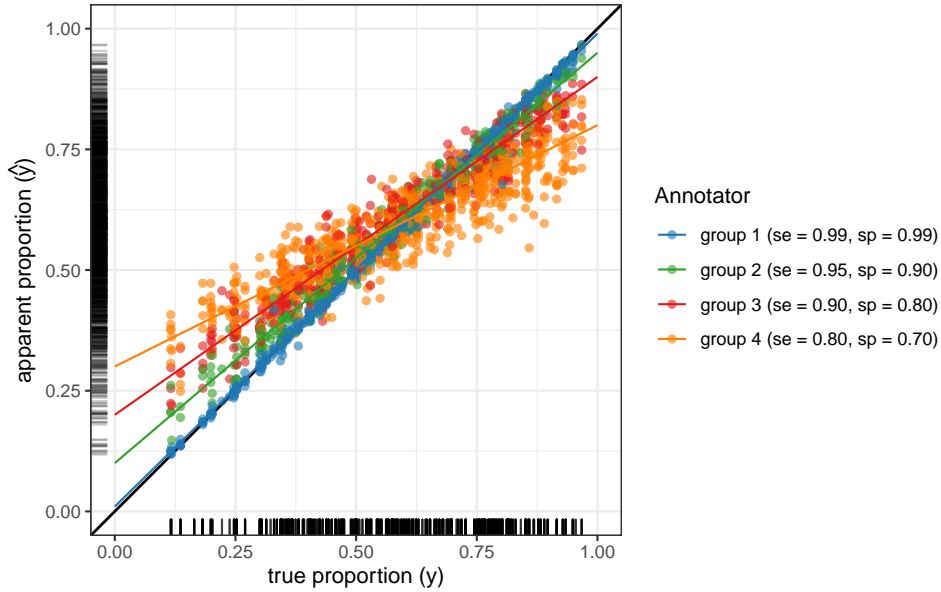


Fig. 9. Apparent proportion (\hat{y}_{ij}) in four groups of users vs the true (y_j) proportion. The black diagonal line represents the ideal case of perfect classification. The lines give the \hat{y}_{ij} for each value of y_j based on the users' mean se_i and sp_i , with points representing the simulated values. Subjects in group 1 have mean $se = 0.99$, $sp = 0.99$; subjects in 2 have $se = 0.95$, $sp = 0.90$; subjects in 3 have $se = 0.90$, $sp = 0.80$; and subjects in 4 have $se = 0.80$, $sp = 0.70$. In all of groups the precision $\phi_{se} = 50$ and $\phi_{sp} = 50$.

(c) contains the estimated values of y_j , which resembles the true latent pattern from (a). The posterior distributions of y_j in 220 cells out of 225 (97.78%) fall within the 95% highest density interval, which shows a suitable coverage of these estimates. Equally the true latent class is well retrieved in 31 of out of 45 unsampled locations, (text in blue color) comparing (c) with (a).

Accounting for misclassification errors allows us to correct the bias in \hat{y}_{ij} and obtain suitable estimates of y_j (Fig. 13). In this figure the red dots are the original \hat{y}_{ij} values obtained from the subjects' classifications. The green dots are the estimated values of y_j when we account for misclassification errors.

A good identification is achieved, with a large proportion of the green dots falling along the diagonal solid line showing a suitable precision of the estimates. The image identifiers for the 45 unsampled locations from Fig. 8 (b) are shown in black. In these points y_j is estimated from the neighbouring measurements and the covariates. There are a few points where the difference in the y_j and \hat{y}_{ij} values is relatively large due to spatial dependency causing the predicted proportion to be higher or lower than expected (e.g. Fig. 13, point 69).

$$\hat{y}_{ij} = y_j \times se_i + (1 - y_j) \times (1 - sp_i)$$

$$y_j | \alpha_j, \beta_j \sim \text{Beta}(\alpha_j, \beta_j)$$

$$\alpha_j = \mu_j \phi$$

$$\beta_j = -\mu_j \phi + \phi$$

$$\text{logit}(\mu_j) = X_j b + u_j$$

$$u_l | u_t, \tau_u \sim \mathcal{N} \left(\frac{1}{n_l} \sum_{l \sim t} u_t, \frac{1}{\tau_u n_l} \right)$$

$$\mu_j = \text{E}[y_j | \alpha_j, \beta_j]$$

$$\text{Var}(y_j) = \frac{\mu_j(1 - \mu_j)}{(1 + \phi)}$$

Priors

$$b_0 \sim \mathcal{N}(\hat{\mu}_{b_0}, 5) \quad \# \text{ informative prior on the regression coefficient intercept}$$

$$b_1 \sim \mathcal{N}(\hat{\mu}_{b_1}, 5) \quad \# \text{ informative prior on the regression coefficient slope}$$

$$se_i \sim \text{Beta}(\alpha_{se}, \beta_{se}) \quad \# \text{ hierarchical informative prior on the sensitivities}$$

$$sp_i \sim \text{Beta}(\alpha_{sp}, \beta_{sp}) \quad \# \text{ hierarchical informative prior on the specificities}$$

$$\phi \sim \mathcal{N}(20, 5) T[10, 60] \quad \# \text{ prior on the beta distribution precision}$$

$$u_j \sim \text{CAR}(\tau_u, W, D) \quad \# \text{ CAR prior for the spatial model}$$

$$\tau_u \sim \text{Gamma}(0.1, 0.1) \quad \# \text{ precision of the spatial effect (CAR prior)}$$

Fig. 10. Hierarchical SDME model and prior distributions.

$$y_{ij} | \alpha_{ij}, \beta_{ij} \sim \text{Beta}(\alpha_{ij}, \beta_{ij})$$

$$\alpha_{ij} = \mu_j w_i \phi$$

$$\beta_{ij} = -\mu_j w_i \phi + \phi$$

$$\text{logit}(\mu_j) = X_j b + u_j + \varepsilon_j$$

$$u_l | u_t, \tau_u \sim \mathcal{N} \left(\frac{1}{n_l} \sum_{l \sim t} u_t, \frac{1}{\tau_u n_l} \right)$$

$$w_i = 1/acc_i$$

$$\mu_j = \text{E}[y_j | \alpha_j, \beta_j]$$

$$\text{Var}(y_j) = \frac{\mu_j(1 - \mu_j)}{(1 + \phi)}$$

Priors

$$b_0 \sim \mathcal{N}(\mu_{b_0}, 5) \quad \# \text{ informative prior on the regression coefficient intercept}$$

$$b_1 \sim \mathcal{N}(\mu_{b_1}, 5) \quad \# \text{ informative prior on the regression coefficient slope}$$

$$acc_i \sim \text{Beta}(\alpha_{se}, \beta_{se}) \quad \# \text{ hierarchical informative prior on the accuracy}$$

$$\phi \sim \mathcal{N}(20, 5) T[10, 60] \quad \# \text{ prior on the beta distribution precision}$$

$$u_j \sim \text{CAR}(\tau_u, W, D) \quad \# \text{ CAR prior for the spatial model}$$

$$\tau_u \sim \text{Gamma}(0.1, 0.1) \quad \# \text{ precision of the spatial effect (CAR prior)}$$

Fig. 11. Hierarchical weighted model and prior distributions.

Table 2. The true value for each of the model parameters, as well as the summary statistics for their posterior distribution, including the mean, standard error (se_mean), and percentiles. The column se_mean represents the Monte Carlo standard error.

model	param	true value	mean	SE mean	sd	2.5%	25%	50%	75%	97.5%
weighted	b_{0_w}	1	0.909	0.010	0.052	0.813	0.874	0.907	0.942	1.023
weighted	b_{1_w}	-2	-1.488	0.029	0.154	-1.836	-1.573	-1.486	-1.377	-1.217
weighted	ϕ	30	59.909	0.003	0.091	59.677	59.873	59.937	59.974	59.998
weighted	acc_1	0.991	0.993	0.000	0.009	0.968	0.990	0.996	0.999	1.000
weighted	acc_2	0.924	0.916	0.001	0.027	0.860	0.899	0.918	0.935	0.962
SDME	$b_{0_{SDME}}$	1	1.023	0.002	0.091	0.847	0.961	1.021	1.083	1.204
SDME	$b_{1_{SDME}}$	-2	-2.020	0.007	0.230	-2.473	-2.171	-2.020	-1.867	-1.568
SDME	ϕ	30	28.009	0.098	4.450	19.728	24.924	27.834	30.917	37.118
SDME	se_1	0.990	0.991	0.000	0.010	0.963	0.987	0.995	0.998	1.000
SDME	se_2	0.948	0.948	0.000	0.031	0.873	0.931	0.954	0.971	0.990
SDME	sp_1	0.991	0.992	0.000	0.011	0.962	0.988	0.995	0.999	1.000
SDME	sp_2	0.899	0.898	0.001	0.039	0.809	0.875	0.903	0.927	0.961

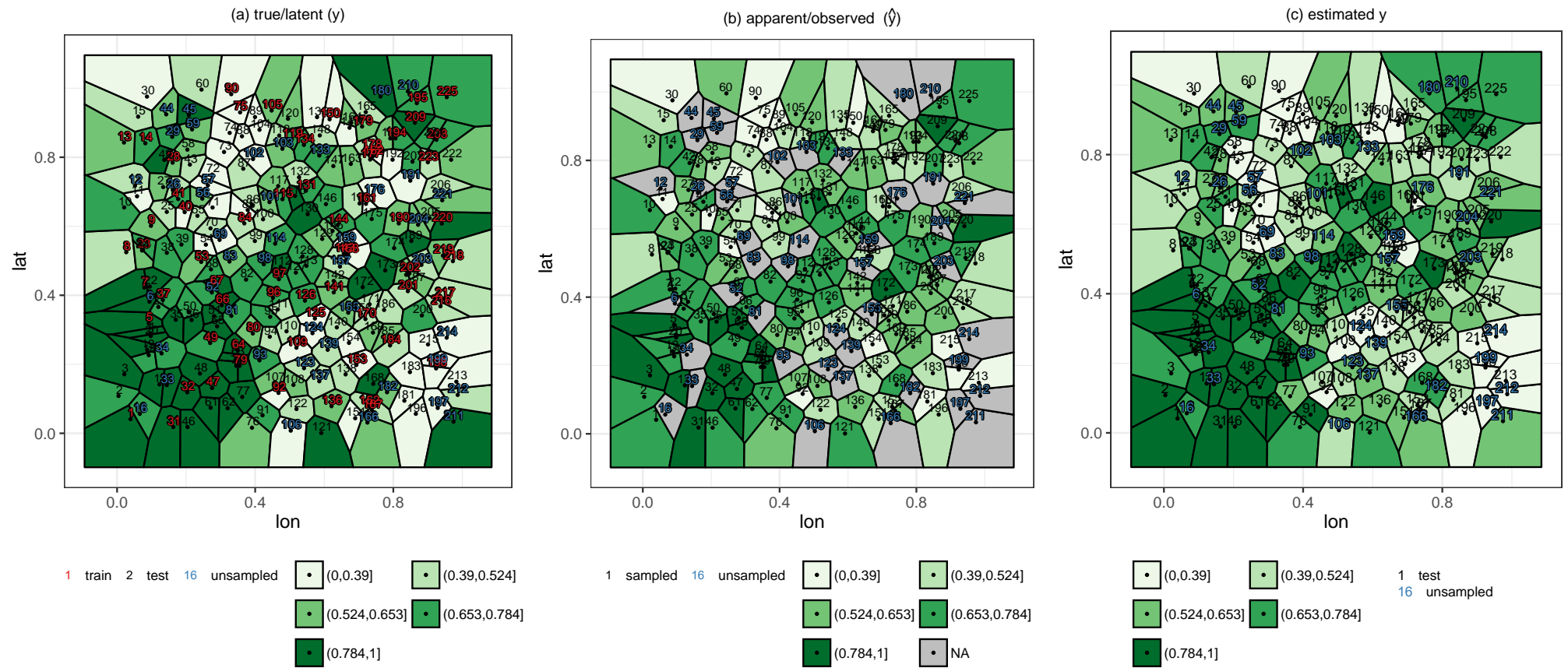


Fig. 12. Voronoi diagram of (a) the true latent proportion y_j at 225 simulated locations, (b) the apparent proportion elicited by subjects (\hat{y}_{ij}), and (c) estimated latent fraction ($y_{\text{estim},j}$). The exact class of the category of y_j is obtained in 199 out of 225 locations. The blue numbers are the cells where values of \hat{y}_{ij} are missing and y_j was predicted solely using the covariate x and neighbouring information.

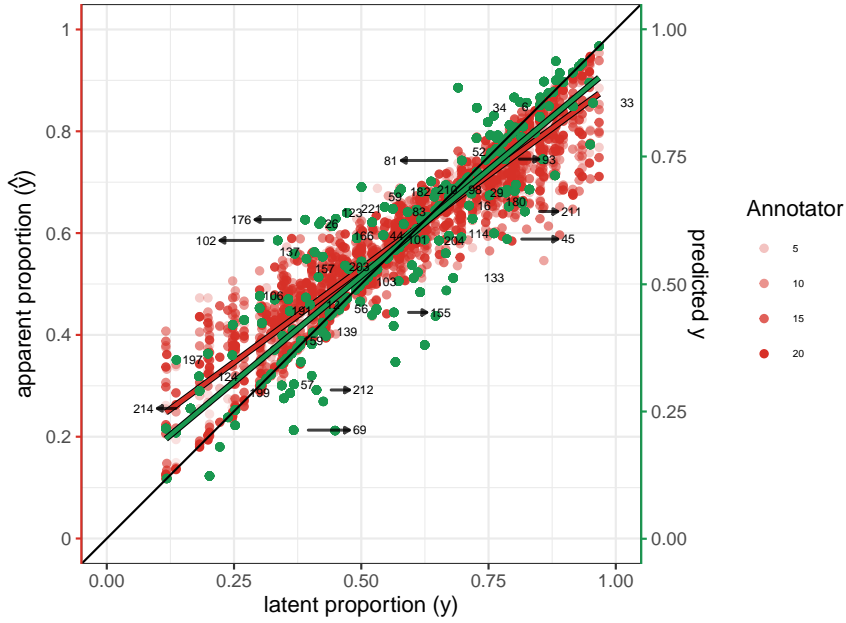


Fig. 13. Bias correction obtained from the spatially dependent misclassification error (SDME) model. The red dots are the elicited \hat{y}_{ij} as a function of the true y_j in the four groups of users (dark red = low se_i and sp_i). The green dots shows the estimated latent variable (y_{estim}) vs y_j after accounting for misclassification errors. The image id of the prediction in 45 unsampled locations from Fig. 8 (b) is also shown. The red and green solid lines are the regression lines from the apparent proportion \hat{y}_{ij} and estimated y_{estim_j} from the model showing how the bias is corrected. The arrows identify the points in the unsampled dataset.

We fitted the weighted and SDME models to each of the 300 simulated datasets and compared how well they retrieved the parameters of interest. The posterior means for the beta regression coefficients suggest that overall the SDME model produced suitable estimates for the regression parameters (Fig. 14). As expected the weighted regression produced more biased regression coefficients than the SDME model, especially for the slope. The SDME model also produced suitable estimates of the subjects' se_i and sp_i values (Fig. 15). However, poor performance measure estimates are obtained from the weighted model.

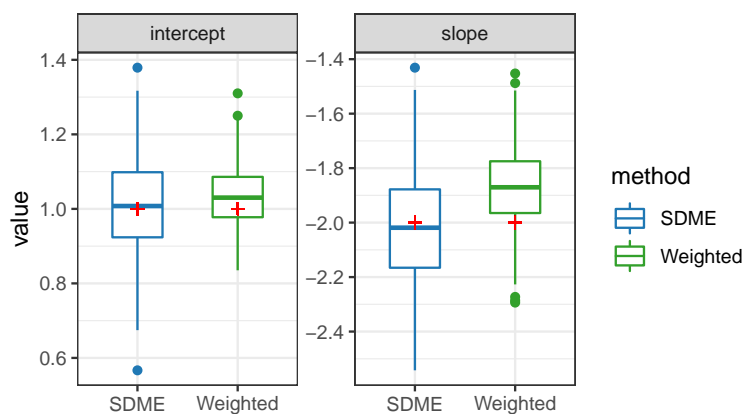


Fig. 14. Boxplots and violin plots of the posterior regression coefficient estimates from weighted and SDME regression models fit to 300 random simulated datasets. The red dots indicate the true parameter values.

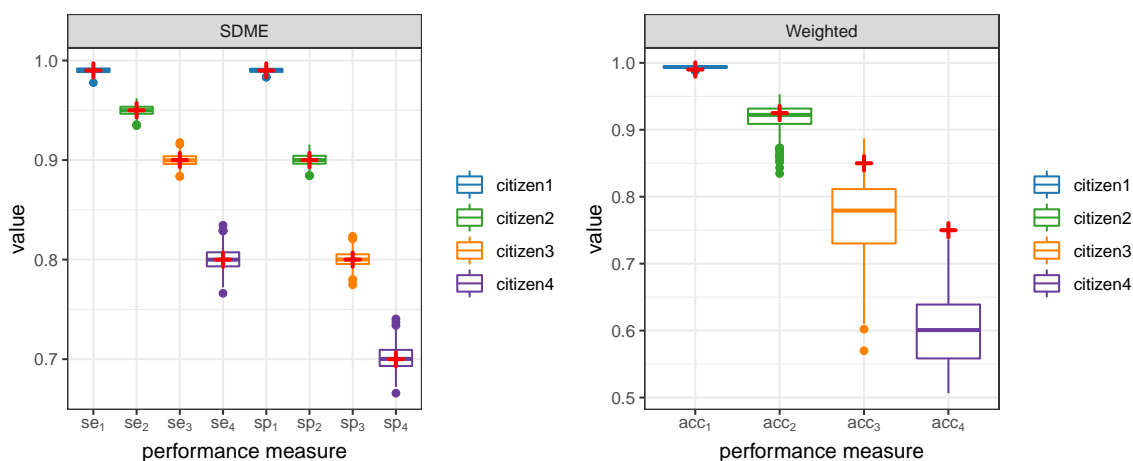


Fig. 15. Boxplots of the posterior performance measures in the SDME (se_i and sp_i) and weighted (acc_i) models for the four groups of subjects in the 300 SDME models. The red crosses indicate the true values.

4. Case study results

We applied the SDME model to coral cover data elicited from underwater images from the GBR. We used the training dataset composed of 171 images to obtain estimates of each subject's se_i and sp_i mean values, which were used to obtain informative priors for the hierarchical model. For example, from Fig. 16 subject 40 classified images 10, 36, 56, 59, 62, 75, etc. Using the classification from the training images (10, 36, 62, 75, etc.) we obtained beta prior distributions for $se_{i=40}$ and $sp_{i=40}$, which were then used to predict the false positive/negative rates. This allowed us to estimate the unknown y_j in the test and unsampled datasets and produce posterior distributions for the se_i and sp_i parameters. In these images, information was also borrowed from the neighbours based on the CAR model and from the four covariates introduced in Section 1.1 Weakly informative priors were also obtained for the regression coefficients from fitting a non-Bayesian beta regression to the data.

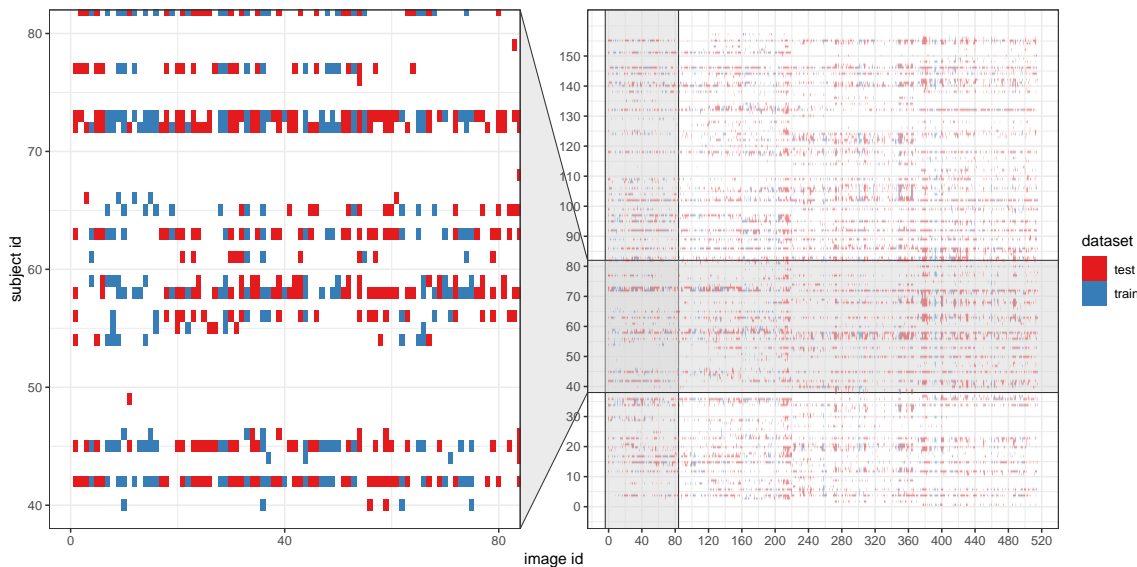


Fig. 16. Images classified per user. The plot on the left shows a subset of the whole dataset, which is shown on the right. Images in red were used as training to learn about the users' performance measures. In the blue images, the underlying true value is unknown and predicted by the model (testing).

The model was fit using Stan on a HPC node with 65 Gb of memory using three processors. We used three chains, a warm-up period of 12,000 samples out of 24,000 iterations and preserving one in three samples (thinning).

Table 3 shows the summary statistics of the posterior distributions for the parameters of interest. The DHW and cyclone impact covariates have a substantial negative effect on the proportion of hard corals, with the 97.5% credible interval well below 0. On the other hand, no-take marine reserves and middle shelf reefs tend to have substantially higher proportions of corals. The posterior densities of the regression coefficients are shown in Fig. 17. These findings are in agreement with several other studies (e.g. Hughes et al., 2018b; Beeden et al., 2015) and demonstrate the capacity of crowdsourced data to answer relevant ecological questions. Fig. 18 shows the latent and the apparent densities y_j and \hat{y}_{ij}

Table 3. Summary statistics of the posterior distribution of the model parameters including the mean, Monte Carlo standard error, standard deviation (sd), and the percentiles. Estimates of the latent variable (y_j) are also given for the first four locations.

parameter	mean	se_mean	sd	2.5%	25%	50%	75%	97.5%
b_{DHW}	-0.136	0.001	0.065	-0.262	-0.179	-0.136	-0.092	-0.007
b_{notake}	0.444	0.004	0.199	0.061	0.310	0.443	0.579	0.836
b_{shelf}	-1.017	0.004	0.176	-1.370	-1.136	-1.015	-0.896	-0.674
$b_{cyclone}$	-0.112	0.000	0.018	-0.147	-0.124	-0.113	-0.100	-0.078
ϕ	10.897	0.100	1.632	10.017	10.190	10.474	11.038	13.998
se_1	0.838	0.001	0.134	0.540	0.748	0.873	0.953	0.998
se_2	0.872	0.001	0.136	0.543	0.789	0.925	0.986	1.000
se_3	0.869	0.001	0.135	0.546	0.787	0.918	0.982	1.000
se_4	0.855	0.001	0.134	0.541	0.771	0.896	0.969	0.999
sp_1	0.902	0.001	0.126	0.567	0.847	0.963	0.997	1.000
sp_2	0.876	0.001	0.128	0.555	0.804	0.922	0.982	1.000
sp_3	0.815	0.001	0.136	0.529	0.714	0.841	0.932	0.995
sp_4	0.787	0.001	0.134	0.526	0.682	0.801	0.901	0.987
y_1	0.346	0.003	0.266	0.002	0.116	0.293	0.535	0.913
y_2	0.310	0.003	0.240	0.003	0.107	0.262	0.470	0.853
y_3	0.382	0.003	0.267	0.006	0.154	0.342	0.583	0.927
y_4	0.374	0.003	0.272	0.003	0.139	0.328	0.581	0.933

respectively and the estimated posterior density of y_j . It shows how well the model corrects the bias in the apparent proportion \hat{y}_{ij} , producing estimates y_j^{pred} quite similar to the latent proportion y_j .

5. Discussion and conclusions

Modern ecological research is relying more and more on citizen science data to learn about latent variables such as the prevalence and abundance of key species and communities (Delaney et al., 2008; van Strien et al., 2013; Bird et al., 2014; Bain, 2016). However, data elicited from citizens is likely to be imprecise and biased (Isaac et al., 2014; Burgess et al., 2017). We present a spatial Bayesian hierarchical model to account for misclassification errors, as well as spatial dependence in the data. The SDME approach can be applied in many other ecological and conservation studies, where citizen scientists are asked to classify images, videos, audio files, etc. For example, in the classification of species presents in videos, the identification birds from audio recordings, etc.

The SDME approach provides a number of benefits over a weighted modelling approach (Table 4). It produces more precise regression coefficient estimates, allows the estimation of the latent variable of interest and accounts for the subjects' abilities. In addition, the case study corroborated results from previous studies, which were obtained using data from professional monitoring programs (Death et al., 2012; Hughes et al., 2018b; Beeden et al., 2015). Although our results did not reveal new ecological relationships, they do suggest that the SDME model can be used to gain a more accurate understanding of the relationships between ecologically meaningful covariates and the response. Despite these

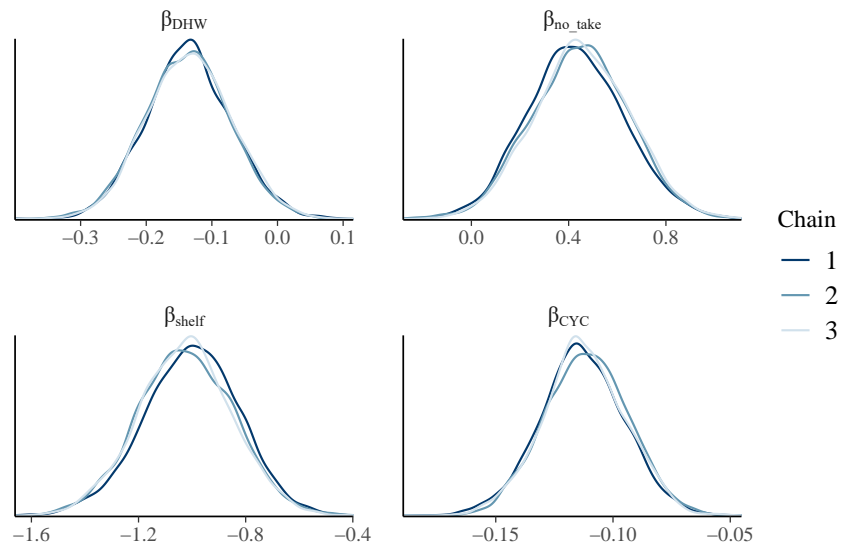


Fig. 17. Posterior densities of the regression coefficients.

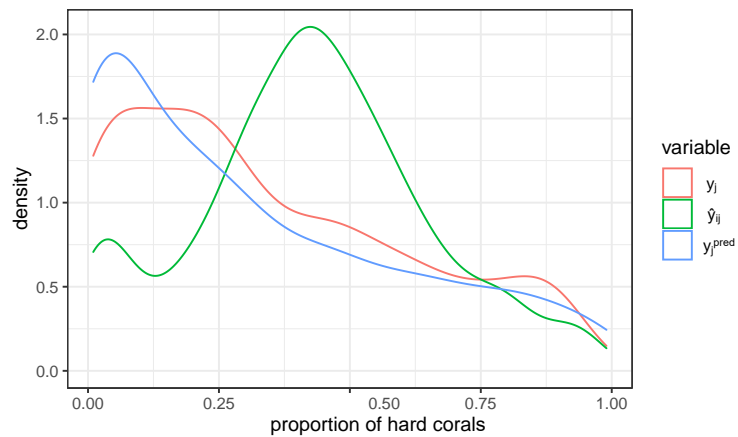


Fig. 18. Density of the true latent proportion of hard corals y_j (in red). The apparent proportion \hat{y}_{ij} and the posterior mean of the predicted proportion $y_{j\text{pred}}$ are shown in green and blue, respectively.

Table 4. Comparison of the weighted regression vs the spatially dependent misclassification error (SDME) model.

Model	benefits	disadvantages
Weighted model	slightly faster	biased regression coefficients
	less parameters to estimate	no estimates of users' abilities or latent variable
		more suitable when users have nearly perfect abilities
SDME model	more precise regression coefficient estimates	more identifiability issues
	accounts for and estimates the users' abilities	more computationally expensive
	produces estimates of the latent response variable	

advantages, there are also limitations to the SDME approach (Table 4).

First, the model is slightly more computationally intensive and becomes prohibitive when the number of locations and elicitations is large (i.e. scalability issues). Second, the SDME model contains a larger number of parameters and as a result, the model cannot be properly identified unless (weakly) informative priors are used for some of them. Finally, both models rely on a large number of classifications per image to ensure that the estimates are robust.

The SDME approach presented here outperformed the weighted approach, but there are other modelling approaches that could also be used. For example, the SDME approach can also be expressed in terms of points containing hard corals rather than a proportion, which can be modelled using discrete distributions such as binomial, Poisson or negative binomial. Similarly, other alternatives for the spatial random effect could be used such as Gaussian random fields or Gaussian processes based on nearest neighbours e.g. Datta et al. (2016); Finley et al. (2017), etc. could be considered. We also explored other approaches for estimating the latent response (y_j). For example, the labels at the point level can be obtained from the majority vote; however, this does not work well for difficult tasks such as those presented in our case study because the probability of answering correctly could be low. Another possible formulation results from rearranging Eq 5 where y_j is directly estimated from the apparent proportion \hat{y}_{ij} , se_i and sp_i . This approach also results in suitable parameter estimates, but requires rather precise se_i and sp_i distributions.

Multiple extensions to the model here discussed can be implemented. For example, we can consider the user's se_i and sp_i distributions to be a mixture, which would be affected by the underlying task difficulty. This is in line with what Chambert et al. (2018) proposed. The false-positive rate tends to be higher when closely related categories are present. Similarly spatio-temporal extensions can be implemented as more images across years become available. In our case study, images were obtained from a professional monitoring program. However, geographical or spatial recording bias should be considered when the data are collected opportunistically (van Strien et al., 2013; Isaac et al., 2014; Mair et al., 2017). Further investigations are also needed to assess whether the results are robust to the way we define the areal units. Another variation could include recursive Bayesian estimation (Särkkä, 2013) in which the model is updated as new data become available. Finally, the integration of coral cover data from CS programs and professional and scientific monitoring programs could also strengthen the model and produce more precise and robust estimates.

R/Stan codes and data used in the study

The R/Stan codes are hosted in https://github.com/EdgarSantos-Fernandez/reef_misclassification. The data used in the case study can be obtained on request from the first author.

Acknowledgement

Thank you to the four reviewers and the editor for their very insightful, detailed and constructive comments, which allowed us to substantially improve the manuscript. The authors declare that they have no conflicts of interest. This research was supported by the Australian Research Council (ARC) Laureate Fellowship Program under the project “Bayesian Learning for Decision Making in the Big Data Era” (ID: FL150100150) and the Centre of Excellence for Mathematical and Statistical Frontiers (ACEMS). Thanks to the members of the VRD team (<https://www.virtualreef.org.au/about/>) in particular to Bryce Christensen. We also thank all the workers that contributed to the classification of images. Ethics approval was obtained from the QUT Human Ethics Advisory Team (Number 1600000830). Some of the computations were performed through the QUT High Performance Computing (HPC) infrastructure. Data analysis and computations were undertaken in R software (R Core Team, 2018) using the packages `rstan` (Stan Development Team, 2018). Data visualizations were made with the packages `tidyverse` (Wickham, 2017), `bayesplot` (Gabry and Mahr, 2018), `ggvoronoi` (Garrett et al., 2018), `ggrepel` (Slowikowski, 2019), and `ggforce` (Pedersen, 2019).

Appendix

Glossary of symbols and definitions

References

- Aarts, G., Fieberg, J. and Matthiopoulos, J. (2012) Comparative interpretation of count, presence–absence and point methods for species distribution models. *Methods in Ecology and Evolution*, **3**, 177–187.
- Ainsworth, T. D., Heron, S. F., Ortiz, J. C., Mumby, P. J., Grech, A., Ogawa, D., Eakin, C. M. and Leggat, W. (2016) Climate change disables coral bleaching protection on the Great Barrier Reef. *Science*, **352**, 338–342.
- Amazon Mechanical Turk () Amazon Mechanical Turk. <https://www.mturk.com/>. Accessed: 2020-01-30.
- Arab, A. and Courter, J. R. (2015) Spatio-temporal trend analysis of spring arrival data for migratory birds. *Communications in Statistics-Simulation and Computation*, **44**, 2535–2547.
- Arab, A., Courter, J. R. and Zelt, J. (2016) A spatio-temporal comparison of avian migration phenology using citizen science data. *Spatial Statistics*, **18**, 234–245.

Table 5. Symbols and definitions

i	subject id, $1, 2, \dots, n$
j	image number, $1, 2, \dots, m$
k	elicitation point, $1, 2, \dots, q$
$z_{ijk} = \{0, 1\}$	indicates if the k^{th} point in the image j was classified as hard coral by the subject i
q	number of elicited points in the image j
$y_j \alpha_j, \beta_j \sim \text{Beta}(\alpha_j, \beta_j)$	true coral cover (latent variable) of the image j
$\alpha_j = \mu_j \phi$	first shape parameter in the beta distribution on the image j
$\beta_j = -\mu_j \phi + \phi$	second shape parameter in the beta distribution on the image j
$\hat{y}_{ij} = y_j \times se_i + (1 - y_j) \times (1 - sp_i)$	apparent coral cover (elicited variable) on the image j by the subject i
$se_i = \frac{\sum_{j=1}^m \sum_{k=1}^q TP_{ijk}}{\sum_{j=1}^m \sum_{k=1}^q TP_{ijk} + \sum_{j=1}^m \sum_{k=1}^q FN_{ijk}}$	sensitivity from the user i
$sp_i = \frac{\sum_{j=1}^m \sum_{k=1}^q TN_{ijk}}{\sum_{j=1}^m \sum_{k=1}^q TN_{ijk} + \sum_{j=1}^m \sum_{k=1}^q FP_{ijk}}$	specificity from the user i
$acc_i = \frac{\sum_{j=1}^m \sum_{k=1}^q TP_{ijk} + \sum_{j=1}^m \sum_{k=1}^q TN_{ijk}}{\sum_{j=1}^m \sum_{k=1}^q TP_{ijk} + \sum_{j=1}^m \sum_{k=1}^q FN_{ijk} + \sum_{j=1}^m \sum_{k=1}^q TN_{ijk} + \sum_{j=1}^m \sum_{k=1}^q FP_{ijk}}$	accuracy from the user i
$TP_{ijk} = \{0, 1\}$	1 if the k^{th} point is a true positive.
$TN_{ijk} = \{0, 1\}$	1 if the k^{th} point is a true negative.
$FP_{ijk} = \{0, 1\}$	1 if the k^{th} point is a false positive.
$FN_{ijk} = \{0, 1\}$	1 if the k^{th} point is a false negative.
b_0	intercept in the regression model
b_1	slope in the regression model
u_j	spatial component (CAR prior) on the image/location j
μ_j	mean of the beta distribution
ϕ	precision parameter in the beta distribution
x	a predictor or disturbances
τ	precision parameter
D	$m \times m$ diagonal matrix
W	$m \times m$ adjacency matrix

- Bachrach, Y., Graepel, T., Minka, T. and Guiver, J. (2012) How to grade a test without knowing the answers-A Bayesian graphical model for adaptive crowdsourcing and aptitude testing. In *Proceedings of the 29th International Conference on Machine Learning, Edinburgh, Scotland, UK*.
- Bain, R. (2016) Citizen science and statistics: Playing a part. *Significance*, **13**, 16–21.
- Beeden, R., Maynard, J., Puotinen, M., Marshall, P., Dryden, J., Goldberg, J. and Williams, G. (2015) Impacts and recovery from severe tropical cyclone yasi on the great barrier reef. *PloS one*, **10**, e0121272.
- Beijbom, O., Edmunds, P. J., Roelfsema, C., Smith, J., Kline, D. I., Neal, B. P., Dunlap, M. J., Moriarty, V., Fan, T.-Y., Tan, C.-J. et al. (2015) Towards automated annotation of benthic survey images: Variability of human experts and operational modes of automation. *PloS one*, **10**, e0130312.
- Bernardo, J. M. and Smith, A. F. (2009) *Bayesian theory*, vol. 405. John Wiley & Sons.
- Besag, J., York, J. and Molli, A. (1991) Bayesian image restoration, with two applications in spatial statistics. *Annals of the Institute of Statistical Mathematics*, **43**, 120.
- Bird, T. J., Bates, A. E., Lefcheck, J. S., Hill, N. A., Thomson, R. J., Edgar, G. J., Stuart-Smith, R. D., Wotherspoon, S., Krkosek, M., Stuart-Smith, J. F., Pecl, G. T., Barrett, N. and Frusher, S. (2014) Statistical solutions for error and bias in global citizen science datasets. *Biological Conservation*, **173**, 144 – 154. URL: <http://www.sciencedirect.com/science/article/pii/S0006320713002693>.
- Bolker, B. M., Brooks, M. E., Clark, C. J., Geange, S. W., Poulsen, J. R., Stevens, M. H. H. and White, J.-S. S. (2009) Generalized linear mixed models: a practical guide for ecology and evolution. *Trends in ecology & evolution*, **24**, 127–135.
- Bonney, R., Shirk, J. L., Phillips, T. B., Wiggins, A., Ballard, H. L., Miller-Rushing, A. J. and Parrish, J. K. (2014) Next steps for citizen science. *Science*, **343**, 1436–1437.
- Burgess, H. K., DeBey, L., Froehlich, H., Schmidt, N., Theobald, E. J., Ettinger, A. K., HilleRisLambers, J., Tewksbury, J. and Parrish, J. K. (2017) The science of citizen science: exploring barriers to use as a primary research tool. *Biological Conservation*, **208**, 113–120.
- Carpenter, B., Gelman, A., Hoffman, M., Lee, D., Goodrich, B., Betancourt, M., Brubaker, M., Guo, J., Li, P. and Riddell, A. (2017) Stan: A probabilistic programming language. *Journal of Statistical Software, Articles*, **76**, 1–32. URL: <https://www.jstatsoft.org/v076/i01>.
- Chambert, T., Grant, E. H. C., Miller, D. A., Nichols, J. D., Mulder, K. P. and Brand, A. B. (2018) Two-species occupancy modelling accounting for species misidentification and non-detection. *Methods in Ecology and Evolution*, **9**, 1468–1477.
- Chambert, T., Miller, D. A. and Nichols, J. D. (2015) Modeling false positive detections in species occurrence data under different study designs. *Ecology*, **96**, 332–339.

- Choy, S. L., O'Leary, R. and Mengersen, K. (2009) Elicitation by design in ecology: using expert opinion to inform priors for bayesian statistical models. *Ecology*, **90**, 265–277.
- Claggett, B., Xie, M. and Tian, L. (2014) Meta-analysis with fixed, unknown, study-specific parameters. *Journal of the American Statistical Association*, **109**, 1660–1671.
- Clare, J. D. J., Townsend, P. A., Anhalt-Depies, C., Locke, C., Stenglein, J. L., Frett, S., Martin, K. J., Singh, A., Van Deelen, T. R. and Zuckerberg, B. (2019) Making inference with messy (citizen science) data: when are data accurate enough and how can they be improved? *Ecological Applications*, **29**, e01849.
- Cribari-Neto, F. and Zeileis, A. (2010) Beta regression in R. *Journal of Statistical Software*, **34**, 1–24. URL: <http://www.jstatsoft.org/v34/i02/>.
- Datta, A., Banerjee, S., Finley, A. O. and Gelfand, A. E. (2016) Hierarchical nearest-neighbor Gaussian process models for large geostatistical datasets. *Journal of the American Statistical Association*, **111**, 800–812.
- Death, G., Fabricius, K. E., Sweatman, H. and Puotinen, M. (2012) The 27-year decline of coral cover on the Great Barrier Reef and its causes. *Proceedings of the National Academy of Sciences*, **109**, 17995–17999.
- Delaney, D. G., Sperling, C. D., Adams, C. S. and Leung, B. (2008) Marine invasive species: validation of citizen science and implications for national monitoring networks. *Biological Invasions*, **10**, 117–128.
- Dickinson, J. L., Zuckerberg, B. and Bonter, D. N. (2010) Citizen science as an ecological research tool: challenges and benefits. *Annual review of ecology, evolution, and systematics*, **41**, 149–172.
- F. Dormann, C., M. McPherson, J., B. Araújo, M., Bivand, R., Bolliger, J., Carl, G., G. Davies, R., Hirzel, A., Jetz, W., Daniel Kissling, W. et al. (2007) Methods to account for spatial autocorrelation in the analysis of species distributional data: a review. *Ecography*, **30**, 609–628.
- Ferrari, S. and Cribari-Neto, F. (2004) Beta regression for modelling rates and proportions. *Journal of Applied Statistics*, **31**, 799–815.
- Finley, A. O., Datta, A., Cook, B. C., Morton, D. C., Andersen, H. E. and Banerjee, S. (2017) Applying nearest neighbor Gaussian processes to massive spatial data sets forest canopy height prediction across Tanana Valley Alaska. *arXiv preprint arXiv:1702.00434*.
- Fithian, W., Elith, J., Hastie, T. and Keith, D. A. (2015) Bias correction in species distribution models: pooling survey and collection data for multiple species. *Methods in Ecology and Evolution*, **6**, 424–438.

- Fritz, S., See, L., Carlson, T., Haklay, M. M., Oliver, J. L., Fraisl, D., Mondardini, R., Brocklehurst, M., Shanley, L. A., Schade, S. et al. (2019) Citizen science and the united nations sustainable development goals. *Nature Sustainability*, **2**, 922–930.
- Fuller, W. A. (2009) *Measurement Error Models*, vol. 305. John Wiley & Sons. New York.
- Gabry, J. and Mahr, T. (2018) *bayesplot: Plotting for Bayesian Models*. URL: <https://CRAN.R-project.org/package=bayesplot>. R package version 1.6.0.
- Garrett, R. C., Nar, A. and Fisher, T. J. (2018) *ggvoronoi: Voronoi Diagrams and Heatmaps with 'ggplot2'*. URL: <https://CRAN.R-project.org/package=ggvoronoi>. R package version 0.8.2.
- Garriga, J., Piera, J. and Bartumeus, F. (2017) A bayesian framework for reputation in citizen science. CEUR Workshop Proceedings.
- GBRMPA (2014) Great Barrier Reef (GBR) features (reef boundaries, QLD mainland, islands, cays, rocks, and dry reefs) shapefile. Great Barrier Reef Marine Park Authority GeoPortal. URL: <https://eatlas.org.au/data/uuid/ac8e8e4f-fc0e-4a01-9c3d-f27e4a8fac3c>.
- GBRMPA (2014) Great Barrier Reef outlook report 2014. Great Barrier Reef Marine Park Authority.
- Gelfand, A. E., Schmidt, A. M., Wu, S., Silander Jr, J. A., Latimer, A. and Rebelo, A. G. (2005) Modelling species diversity through species level hierarchical modelling. *Journal of the Royal Statistical Society: Series C (Applied Statistics)*, **54**, 1–20.
- Gelman, A., Rubin, D. B. et al. (1992) Inference from iterative simulation using multiple sequences. *Statistical science*, **7**, 457–472.
- Gold, C. (2016) Spatial modeling: V oronoi diagrams. *International Encyclopedia of Geography: People, the Earth, Environment and Technology: People, the Earth, Environment and Technology*, 1–24.
- González-Rivero, M., Bongaerts, P., Beijbom, O., Pizarro, O., Friedman, A., Rodriguez-Ramirez, A., Upcroft, B., Laffoley, D., Kline, D., Bailhache, C. et al. (2014) The Catlin Seaview Survey—kilometre-scale seascape assessment, and monitoring of coral reef ecosystems. *Aquatic Conservation: Marine and Freshwater Ecosystems*, **24**, 184–198.
- Guélat, J. and Kéry, M. (2018) Effects of spatial autocorrelation and imperfect detection on species distribution models. *Methods in Ecology and Evolution*, **9**, 1614–1625.
- Higgins, J. P., Thompson, S. G. and Spiegelhalter, D. J. (2009) A re-evaluation of random-effects meta-analysis. *Journal of the Royal Statistical Society: Series A (Statistics in Society)*, **172**, 137–159.
- Hobbs, N. T. and Hooten, M. B. (2015) *Bayesian models: a statistical primer for ecologists*. Princeton University Press.

- Hoffman, M. D. and Gelman, A. (2014) The No-U-turn sampler: adaptively setting path lengths in Hamiltonian Monte Carlo. *Journal of Machine Learning Research*, **15**, 1593–1623.
- Hsu, A., Malik, O., Johnson, L. and Esty, D. C. (2014) Development: Mobilize citizens to track sustainability. *Nature News*, **508**, 33.
- Hughes, T. P., Anderson, K. D., Connolly, S. R., Heron, S. F., Kerry, J. T., Lough, J. M., Baird, A. H., Baum, J. K., Berumen, M. L., Bridge, T. C. et al. (2018a) Spatial and temporal patterns of mass bleaching of corals in the anthropocene. *Science*, **359**, 80–83.
- Hughes, T. P., Kerry, J. T., Baird, A. H., Connolly, S. R., Dietzel, A., Eakin, C. M., Heron, S. F., Hoey, A. S., Hoogenboom, M. O., Liu, G. et al. (2018b) Global warming transforms coral reef assemblages. *Nature*, **556**, 492.
- Humphreys, J. M., Murrow, J. L., Sullivan, J. D. and Prosser, D. J. (2019) Seasonal occurrence and abundance of dabbling ducks across the continental united states: Joint spatio-temporal modelling for the genus *anas*. *Diversity and Distributions*.
- Isaac, N. J., van Strien, A. J., August, T. A., de Zeeuw, M. P. and Roy, D. B. (2014) Statistics for citizen science: extracting signals of change from noisy ecological data. *Methods in Ecology and Evolution*, **5**, 1052–1060.
- Jordan, R. C., Gray, S. A., Howe, D. V., Brooks, W. R. and Ehrenfeld, J. G. (2011) Knowledge gain and behavioral change in citizen-science programs. *Conservation Biology*, **25**, 1148–1154.
- Kohler, K. E. and Gill, S. M. (2006) Coral point count with excel extensions (cpce): A visual basic program for the determination of coral and substrate coverage using random point count methodology. *Computers & Geosciences*, **32**, 1259–1269.
- Koricheva, J., Gurevitch, J. and Mengersen, K. (2013) *Handbook of meta-analysis in ecology and evolution*. Princeton University Press.
- Kosmala, M., Wiggins, A., Swanson, A. and Simmons, B. (2016) Assessing data quality in citizen science. *Frontiers in Ecology and the Environment*, **14**, 551–560.
- Lichstein, J. W., Simons, T. R., Shriener, S. A. and Franzreb, K. E. (2002) Spatial autocorrelation and autoregressive models in ecology. *Ecological monographs*, **72**, 445–463.
- Mair, L., Harrison, P. J., Jönsson, M., Löbel, S., Nordén, J., Siitonen, J., Lämås, T., Lundström, A. and Snäll, T. (2017) Evaluating citizen science data for forecasting species responses to national forest management. *Ecology and evolution*, **7**, 368–378.
- Manel, S., Williams, H. C. and Ormerod, S. J. (2001) Evaluating presence–absence models in ecology: the need to account for prevalence. *Journal of applied Ecology*, **38**, 921–931.

- Marshall, N. J., Kleine, D. A. and Dean, A. J. (2012) Coralwatch: education, monitoring, and sustainability through citizen science. *Frontiers in Ecology and the Environment*, **10**, 332–334.
- Matthews, S. A., Mellin, C., MacNeil, A., Heron, S. F., Skirving, W., Puotinen, M., Devlin, M. J. and Pratchett, M. (2019) High-resolution characterization of the abiotic environment and disturbance regimes on the great barrier reef, 1985–2017. *Ecology*, **100**, e02574.
- McClanahan, T. R., Darling, E. S., Maina, J. M., Muthiga, N. A., Dagata, S., Jupiter, S. D., Arthur, R., Wilson, S. K., Mangubhai, S., Nand, Y. et al. (2019) Temperature patterns and mechanisms influencing coral bleaching during the 2016 el niño. *Nature Climate Change*, **9**, 845–851.
- Mellin, C., Thompson, A., Jonker, M. J. and Emslie, M. J. (2019) Cross-shelf variation in coral community response to disturbance on the great barrier reef. *Diversity*, **11**, 38.
- Mengersen, K., Peterson, E. E., Clifford, S., Ye, N., Kim, J., Bednarz, T., Brown, R., James, A., Vercelloni, J., Pearce, A. R., Davis, J. and Hunter, V. (2017) Modelling imperfect presence data obtained by citizen science. *Environmetrics*, **28**, e2446. URL: <https://onlinelibrary.wiley.com/doi/abs/10.1002/env.2446>. E2446 env.2446.
- Morris, M., Wheeler-Martin, K., Simpson, D., Mooney, S. J., Gelman, A. and DiMaggio, C. (2019) Bayesian hierarchical spatial models: Implementing the besag york molli model in stan. *Spatial and Spatio-temporal Epidemiology*, **31**, 100301. URL: <http://www.sciencedirect.com/science/article/pii/S1877584518301175>.
- Muff, S., Riebler, A., Held, L., Rue, H. and Saner, P. (2015) Bayesian analysis of measurement error models using integrated nested Laplace approximations. *Journal of the Royal Statistical Society: Series C (Applied Statistics)*, **64**, 231–252.
- Nichols, J. D. and Williams, B. K. (2006) Monitoring for conservation. *Trends in ecology & evolution*, **21**, 668–673.
- Nygård, H., Oinonen, S., Hallfors, H. A., Lehtiniemi, M., Rantajarvi, E. and Uusitalo, L. (2016) Price vs. value of marine monitoring. *Frontiers in Marine Science*, **3**, 205.
- Okabe, A., Boots, B., Sugihara, K. and Chiu, S. N. (2009) *Spatial tessellations: concepts and applications of Voronoi diagrams*, vol. 501. John Wiley & Sons.
- Pacifici, K., Reich, B. J., Miller, D. A., Gardner, B., Stauffer, G., Singh, S., McKerrow, A. and Collazo, J. A. (2017) Integrating multiple data sources in species distribution modeling: A framework for data fusion. *Ecology*, **98**, 840–850.
- Pagel, J., Anderson, B. J., O’Hara, R. B., Cramer, W., Fox, R., Jeltsch, F., Roy, D. B., Thomas, C. D. and Schurr, F. M. (2014) Quantifying range-wide variation in population trends from local abundance surveys and widespread opportunistic occurrence records. *Methods in Ecology and Evolution*, **5**, 751–760.

- Pedersen, T. L. (2019) *ggforce: Accelerating “ggplot2”*. URL: <https://CRAN.R-project.org/package=ggforce>. R package version 0.2.2.
- Peterson, E. E., Santos-Fernández, E., Chen, C., Clifford, S., Vercelloni, J., Pearse, A., Brown, R., Christensen, B., James, A., Anthony, K. et al. (2020) Monitoring through many eyes: Integrating disparate datasets to improve monitoring of the great barrier reef. *Environmental Modelling & Software*, **124**, 104557.
- Petracca, L. S., Frair, J. L., Cohen, J. B., Calderón, A. P., Carazo-Salazar, J., Castañeda, F., Corrales-Gutiérrez, D., Foster, R. J., Harmsen, B., Hernández-Potosme, S. et al. (2018) Robust inference on large-scale species habitat use with interview data: The status of jaguars outside protected areas in central america. *Journal of applied ecology*, **55**, 723–734.
- Puotinen, M., Maynard, J. A., Beeden, R., Radford, B. and Williams, G. J. (2016) A robust operational model for predicting where tropical cyclone waves damage coral reefs. *Scientific reports*, **6**, 26009.
- Purse, B. V., Comont, R., Butler, A., Brown, P. M., Kessel, C. and Roy, H. E. (2015) Landscape and climate determine patterns of spread for all colour morphs of the alien ladybird *harmonia axyridis*. *Journal of Biogeography*, **42**, 575–588.
- R Core Team (2018) *R: A Language and Environment for Statistical Computing*. R Foundation for Statistical Computing, Vienna, Austria. URL: <https://www.R-project.org/>.
- Rashtchian, C., Young, P., Hodosh, M. and Hockenmaier, J. (2010) Collecting image annotations using amazon’s mechanical turk. In *Proceedings of the NAACL HLT 2010 Workshop on Creating Speech and Language Data with Amazon’s Mechanical Turk*, 139–147. Association for Computational Linguistics.
- Rice, K., Higgins, J. P. and Lumley, T. (2018) A re-evaluation of fixed effect (s) meta-analysis. *Journal of the Royal Statistical Society: Series A (Statistics in Society)*, **181**, 205–227.
- Roelfsema, C., Kovacs, E., Ortiz, J. C., Wolff, N. H., Callaghan, D., Wettle, M., Ronan, M., Hamylton, S. M., Mumby, P. J. and Phinn, S. (2018) Coral reef habitat mapping: A combination of object-based image analysis and ecological modelling. *Remote sensing of environment*, **208**, 27–41.
- Roelfsema, C. and Phinn, S. (2010) Calibration and validation of coral reef benthic community maps derived from high spatial resolution satellite imagery. *Journal of Applied Remote Sensing*, **4**, 043527.
- Särkkä, S. (2013) *Bayesian filtering and smoothing*, vol. 3. Cambridge University Press.
- Slowikowski, K. (2019) *ggrepel: Automatically Position Non-Overlapping Text Labels with ‘ggplot2’*. URL: <https://CRAN.R-project.org/package=ggrepel>. R package version 0.8.1.
- Stan Development Team (2018) RStan: the R interface to Stan. URL: <http://mc-stan.org/>. R package version 2.18.2.

- van Strien, A. J., van Swaay, C. A. and Termaat, T. (2013) Opportunistic citizen science data of animal species produce reliable estimates of distribution trends if analysed with occupancy models. *Journal of Applied Ecology*, **50**, 1450–1458.
- Sullivan, B. L., Wood, C. L., Iliff, M. J., Bonney, R. E., Fink, D. and Kelling, S. (2009) ebird: A citizen-based bird observation network in the biological sciences. *Biological Conservation*, **142**, 2282–2292.
- US Federal (2018) Crowdsourcing and Citizen Science Toolkit. <https://www.citizenscience.gov/toolkit/>. Accessed:2019-01-14.
- Vayssières, M. P., Plant, R. E. and Allen-Diaz, B. H. (2000) Classification trees: An alternative non-parametric approach for predicting species distributions. *Journal of vegetation science*, **11**, 679–694.
- Vehtari, A., Gelman, A., Simpson, D., Carpenter, B. and Bürkner, P.-C. (2019) Rank-normalization, folding, and localization: An improved \widehat{R} for assessing convergence of mcmc. *arXiv preprint arXiv:1903.08008*.
- Venanzi, M., Guiver, J., Kazai, G., Kohli, P. and Shokouhi, M. (2014) Community-based Bayesian aggregation models for crowdsourcing. In *Proceedings of the 23rd international conference on World Wide Web*, 155–164. ACM.
- Ver Hoef, J. M., Peterson, E. E., Hooten, M. B., Hanks, E. M. and Fortin, M.-J. (2018) Spatial autoregressive models for statistical inference from ecological data. *Ecological Monographs*, **88**, 36–59.
- Vercelloni, J., Liqueur, B., Kennedy, E. V., Gonzalez-Rivero, M., Caley, M. J., Peterson, E. E., Puotinen, M., Hoegh-Guldberg, O. and Mengersen, K. (2020) Forecasting intensifying disturbance effects on coral reefs. *Global Change Biology*, **26**, 2785–2797. URL: <https://onlinelibrary.wiley.com/doi/abs/10.1111/gcb.15059>.
- Vose, D. (2008) *Risk analysis: A quantitative guide*. John Wiley & Sons New York, 3. ed. edn.
- Wickham, H. (2017) *tidyverse: Easily Install and Load the 'Tidyverse'*. URL: <https://CRAN.R-project.org/package=tidyverse>. R package version 1.2.1.
- Wiggins, A. and Crowston, K. (2015) Surveying the citizen science landscape. *First Monday*, **20**.

Table 6. Regression model, if the latent variable were observed directly or not there is no misclassification

	Estimate	Std. Error	z value	Pr(> z)
(Intercept)	-4.96275	0.09144	-54.27365	0.00000
x	9.92043	0.16941	58.55978	0.00000

Supplementary materials

6. Example of a beta regression in presence of misclassification

In this example, we illustrate how misclassification in the response variable produces biased regression coefficients. We simulate a dataset comprising 200 observations with a covariate ($x \sim \text{Uni}(0, 1)$) and a response variable that is beta distributed ($y \sim \text{Beta}(\alpha, \beta)$). The response y is not directly observed but obtained from the elicited variable \hat{y} produced from image classification. Consider four users ($i = 1, \dots, 4$) with different performance measures being $se_i = sp_i = \{0.90, 0.80, 0.70, 0.60\}$.

```
# R codes
set.seed(201901)
n <- 200          # sample size
x <- runif(n, 0, 1) # a covariate
beta <- c(-5, 10) # fixing regression coefficients

mu <- -1 / (1 + exp(-(beta[1] + beta[2] * x))) # mean
phi = 50        # precision
a = mu * phi    # shape 1
b = -mu * phi + phi # shape 2
y = rbeta(n, a, b) # response variable

df <- data.frame(x = x, y = y)

annot <- rep( c('cit1', 'cit2', 'cit3', 'cit4'), each = 50)
df$annot <- sample(annot, size = nrow(df), replace = FALSE)

perf <- data.frame(annot = c('cit1', 'cit2', 'cit3', 'cit4'),
  se = c(0.90, 0.80, 0.70, 0.60))
df <- merge(df, perf, by = 'annot')
df$yhat <- (df$y * df$se + (1 - df$y) * (1 - df$se))
# the apparent prop (apparent coral cover).
# For simplicity let us assume se = sp
```

If the latent variable y were observed directly we can retrieve the fixed regression coefficients well (Table 6)

```
library("betareg")
m <- betareg(y ~ x, data = df) # model for the true fraction
summary(m)$coefficients$mean
```

Table 7. Ignoring the misclassification

	Estimate	Std. Error	z value	Pr(> z)
(Intercept)	-1.47758	0.06734	-21.94303	0.00000
x	2.91030	0.11394	25.54236	0.00000

Table 8. Accounting for misclassification using weights

	Estimate	Std. Error	z value	Pr(> z)
(Intercept)	-1.58172	0.07937	-19.92916	0.00000
x	3.11236	0.13495	23.06243	0.00000

Ignoring the misclassification problem:

We obtain very poor estimates when the regression is performed directly from the observed apparent variable \hat{y} (Table 7).

```
m1 <-betareg(yhat ~x, data = DF) # model for the apparent fraction
(sum1 <-summary(m1)$coefficients$mean)
```

Accounting for misclassification using weights

Using weights proportional to the performance measures yields slightly better estimates compared to the previous model but still very biased intercept and slope estimates (Table 8).

```
m2 <-betareg(yhat ~x, data = df, weights = acc) # model for the apparent fraction
sum2 <-summary(m2)$coefficients$mean
```

Fig19 shows the unobserved true response variable (in gray) and the observed apparent response (in orange).

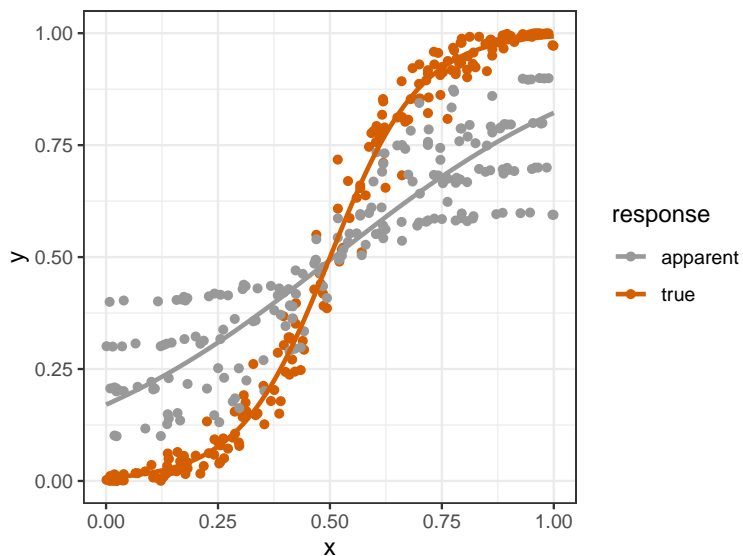


Fig. 19. True unobserved response variable (in gray) and the observed apparent response (in orange) as a function of a predictor x .

7. Posterior densities and trace plots from the simulation study

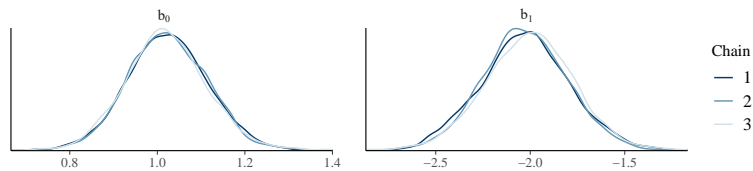


Fig. 20. Posterior densities of the regression coefficients.

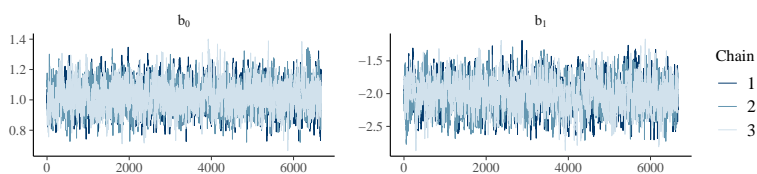


Fig. 21. Trace plots of the regression coefficients.

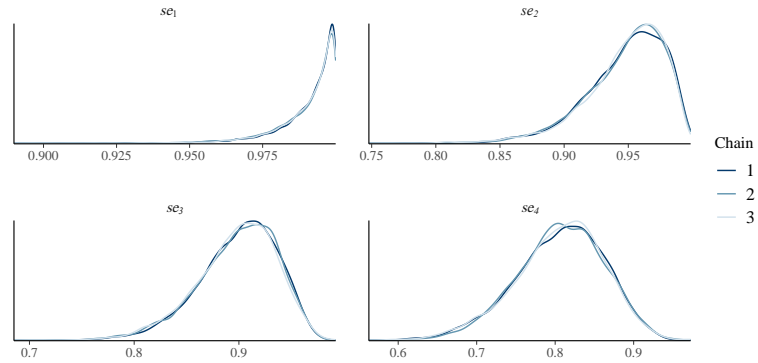


Fig. 22. Posterior densities of the first four subjects' se . The true fixed values are: $se_1 = 0.99$, $se_2 = 0.95$, $se_3 = 0.90$, $se_4 = 0.80$.

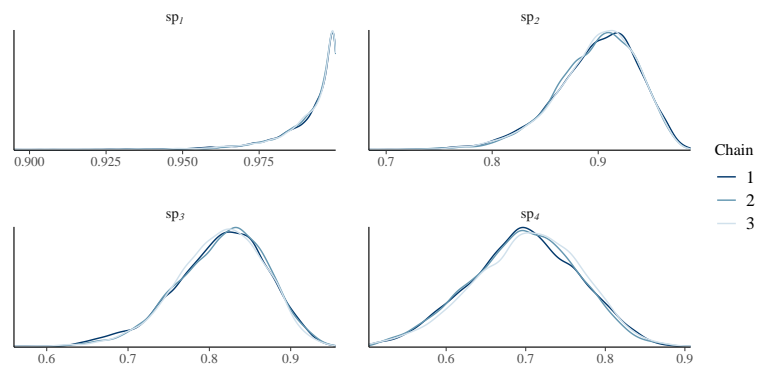


Fig. 23. Posterior densities of the first four subjects' sp . The true values are: $sp_1 = 0.99$, $sp_2 = 0.90$, $sp_3 = 0.80$, $sp_4 = 0.70$.